Response to the comments of reviewer#1

The Voronoi model is compared to pristine hexagonal columns, plates, bullet-rosettes and droxtals. Already since the first POLDER publications in the 1990s that also used the SAD method, in addition to analysis of polarized reflectances, it is clear that pristine crystals with hexagonal parts are inconsistent with the measurements. Basically all the papers referred to on page 31669, line 21-23, and page 31670, line 5-6, come to this conclusion. Including pristine crystals in the analysis performed here is therefor pointless. Since discussion of the pristine models compared with the Voronoi model takes up most of the paper, either that analysis needs to be repeated with rough models or in my opinion the paper should be rejected in the current form. In figure 10, the rough 5-plate aggregate is shown. I assume the optical properties for that habit are obtained from the Yang et al. database. The authors may want to use the optical properties of other rough particles in that database instead of their own calculations. Otherwise, a shorter paper just focusing on the Voronoi particles may be suited for publication.
Aside from this main comment, there are various other major shortcomings in this paper, as well as some minor issues. Below my other major and minor comments are listed. Should the paper be accepted in some form, I recommend these issues to be addressed. Both the conclusions and the abstract should also be revised accordingly.

Answer: The reason for using hexagonal column, plates, bullet rosettes, and droxtal habits in this study is to provide a sense of different optical properties and to determine the optimal habit model used in the ice cloud retrievals. As the reviewer mentioned, some pristine models employed in this study were already investigated in previous studies. We have reduced the description about the pristine models in the manuscript. However, I don't think it is a full replication of previous studies to include the results for pristine models because compared to previous studies we have more data processed and in a fully consistent manner so it does make sense in my view to keep the results for the other pristine models even if we emphasize and focus on the results obtained for the Voronoi. It can easily be justified that we want to maintain other results in the paper because it is the first publication that compares all models in a consistent way for the exact same observation dataset. Even if previous studies came to the same conclusion, it reinforces our analysis and provides a reliable basis for discussing the Voronoi model. So we want to reduce the discussion of the pristine models but still keep those in the current paper for full reference.

Major comments:

1) A model is searched to be used for optical thickness and size retrievals using the commonly used Nakajima-King approach as illustrated in Fig. 6. Such an approach requires the optical properties to be integrated over size distributions as shown by Baum et al. (2005). The authors define an effective radius in Eq 6., where a size distribution is used, although not specified. However, in their SAD analysis, as far as I understand, only single particle optical properties are used. To be consistent with their goal, I recommend using size-distribution integrated optical properties for the SAD analysis. It should be specified which size distributions are used. The conclusion that small bullet rosettes are consistent with the data is because these tiny crystals have size parameters well below 100 and therefore smooth phase functions. However, the contribution of these small particles to scattering properties for any realistic size distribution is probably negligible. Thus, I expect only the Voronoi model to be consistent with the measurements once size distributions are used, since the other models are pristine and have phase functions with features. Furthermore, it should be pointed out that for particle size retrievals, a model is needed that is consistent with measurements over a large range of sizes

and not just a single size.

Answer: According to the suggestions, we have performed the size distribution integrated optical properties on the SGLI scattering habit models as shown by Baum et al., (2005, 2011) for the SAD analysis (Please see line 5 page 7 to line 6, page 8).

The particle size distribution (PSD) of the effective radius defined by Nakajima and Nakajima (1995, JAS) is used for simulating the data in Figure 6. The RSTAR radiative transfer model (Nakajima et al. 1986, 1988 and Sekiguchi et al. 2008) with single scattering properties database for various ice habit models is employed to simulate the graph in Figure 6 (in the last submitted version).

In this study, we aim to investigate the optimal ice particle habit using SAD analysis. However, as the reviewer mentioned, there are some inconsistent between description of the single particle scattering property and size-distribution integrated optical properties as shown in Eq.3 to Eq.6 (in the previous version). In order to avoid the confusion, we have modified Eq. 3 and Eq. 6 based on the Baran et al. (2006). As a future study, we are going to investigate the optical thickness and size retrievals for various habit models based on the Nakajima-King approach as showing in Figure 6. So, we decided to remove Figure 6 from the current version of the manuscript.

In this study, except for Voronoi habit, various sizes of the hexagonal column, plates, bullet rosettes, and droxtal habits were chosen simply to provide a sense of different optical properties. The reason for using the various size of bullet rosettes is not only for investigating the shape of the bullet rosettes, but also for investigating whether the optical property of the bullet rosettes habits with varying size can satisfy the SAD measurements.

Reference:

Nakajima, T., and M. Tanaka, 1986: Matrix formulations for the transfer of solar radiation in a plane-parallel scattering atmosphere. J. Quant. Spectrosc. Radiat. Transfer, 35, 13-21.

Nakajima, T., and M. Tanaka, 1988: Algorithms for radiative intensity calculations in moderately thick atmospheres using a truncation approximation. J. Quant. Spectrosc. Radiat. Transfer , 40, 51-69.

Sekiguchi, Miho, and Teruyuki Nakajima. "A k-distribution-based radiation code and its computational optimization for an atmospheric general circulation model." Journal of Quantitative Spectroscopy and Radiative Transfer 109.17 (2008): 2779-2793.

2) Several definitions are unclear in the paper. On page P316672, $\bar{r}$ is named the effective radius, but it is defined as the radius of an equivalent volume sphere. Effective radius for a single particle is usually defined as three-fourth of the volume over the projected area, which is a relevant size definition for determining the single scattering albedo. Using the term “effective radius” for r^ is confusing and should be avoided. I suggest to name r^ “volume-equivalent radius”.

Answer: In order to avoid the confusion, we have used the name re “volume-equivalent radius” instead of “effective radius” according to the suggestions.

In equation 6, a size-integrated effective radius is defined, which adds to this confusion as it is unclear which “effective radius” is meant in the following parts of the paper. Furthermore, the

effective radius defined in Eq. 6 is based on the size distribution weighted integration of r^3 and r^2. If I am correct this is not consistent with the usual definition of effective radius for non-spherical ice, which is three-fourth of the total volume over the total project area. Please use the common definition of effective radius or rename it and use a symbol other than re.

For the calculation of effective radius as defined in eq. 6, size distributions are needed. What size distributions are used here? For non-spherical particles it is not trivial to choose a size distribution to obtain a specific effective radius (as it is for spheres). For example, this problem was described and tackled by Baum et al. (2005, 2011) by applying about 14000 size distributions and sorting them for effective radius afterwards. It seems that here re is only used for figure 6 in the current version, but the authors should discuss the size distributions applied as also remarked in my previous comment.

Answer: As the reviewer pointed out, the calculation of effective radius as defined in Eq. 6 is not consistent with Re in Eq. 4 (in the previous version). Thus, we have modified the Eq. 6 based on the paper by Baum et al (2005,1011). Furthermore, we have removed Fig. 6 from the manuscript (The reason is descripted in answer 1).

On page 31679, the comparison to other models from "conventional studies" is described. The optical properties of GHM model are provided by Bryan Baum. If I am correct, the optical properties available for the GHM are already integrated over size distributions and are given for specific effective radius (defined in the traditional way). However, here the authors say they compare the model using a single particle equivalent volume radius r^ of 30 micron. I doubt that this is correct. Although this may not matter much for the analysis, it is all very confusing and inconsistent.

Answer: According to the suggestions, we have performed the size-distribution integrated optical properties on the SGLI habit models based on the Baum et al., (2005, 2011) for the SAD analysis in the revised manuscript. In the improved version, we employed the effective diameter (D_{eff} =60 micron) for calculating the bulk scattering properties of the SGLI models instead of equivalent volume radius r^ of 30 micron.

3) The calculations for the SAD analysis are very unclear. Equation 3 on P316674 is technically incorrect. The right part is an observed quantity, while the left part is a modeled quantity since the τ, re, ω and P11 dependency is included. In the following it is very unclear what is modeled and what is measured. The SAD analysis compares measurements with simulations, but nowhere in these equations there is a difference taken between measurements and simulations. Also, the step-wise description on page P316674-75 suggests that this is applied on a pixel-by pixel basis, while the model evaluation is done on globally, temporally averaged data. The SAD analysis is probably better explained in some previous Baran et al. papers, so I suggest to correct the equations and description based on such previous work.
It should also be pointed out that simulated R_{cld} is a function of τ, ω and P11, but then not also of re. The re dependency of R_{cld} comes from the dependency of ω and P11 on re.

Answer: According to the suggestion, we have modified Eq. 3 in the manuscript based on the paper by Baran et al., (2006). (Please see line1-25, page 9)

In line1-25, page 9:

"For calculating the cloud spherical albedo, bi-directional reflection is first determined by

$$R_{cld}(\mu, \mu_0, \phi - \phi_0) = \pi L_{obs}(\mu, \mu_0, \phi - \phi_0)/\mu_0 F_0 \,, \qquad (9)$$

where u, and u_0 are cosines of the satellite and solar zenith angles, $\phi - \phi_0$ is the relative azimuth angle between the satellite and the sun, L_{obs} is the reflected solar radiance observed by the satellite, and F_0 is the solar flux density. Cloud-plane albedo (A_p) and spherical albedo (S) are calculated by integrating over all the zenith and azimuth angles as

$$A_p(\mu_0) = \iint R_{cld}(\mu, \mu_0, \phi - \phi_0)\mu d\mu d\phi, \quad (10)$$
$$S = \int A_p(\mu_0)\mu_0 d\mu_0, \quad (11)$$

The value of cloud spherical albedo ($S(\theta)$) can be calculated from the L_{obs} in each pixel of the POLDER measurements with various scattering angles (θ) to investigate the P_{11} element of the ice particle models. The total observation number (N) of L_{obs} with various θ values is up to 16, and is limited to the viewing geometries of the measurements. Baran et al. (2006) assumed that if the scattering phase function of the ice particle model is correct, then calculated $S(\theta)$ in each direction should be the same and the SAD, as shown in Eq. (13), should be 0. $\bar{S}$, SAD, and θ are given as

$$\bar{S} = (1/N)\sum S(\theta) \quad (12)$$
$$SAD = S(\theta) - \bar{S} \quad (13)$$
$$cos\ \theta\ = cos(\pi - u_0)cos\ u\ +\ sin\ u_0\ sin\ u \cos(\phi - \phi_0), \quad (14)$$

where u_0 and u are the solar and satellite zenith angles, respectively. ”

Aside, the SAD analysis is described here in terms of re, while the applied SAD analysis is in terms of r^. This should be made consistent. As pointed out in my previous comment, the SAD analysis should also be performed using size-integrated phase function.

Answer: According to the suggestion, we have re-analyzed the SAD analysis by applying the size-integrated phase function. In the current version of the manuscript, we employed the effective diameter (D_{eff} =60 micron) for calculating the bulk scattering properties of the SGLI models instead of equivalent volume radius r^ based on the Baum et al., (2011).

In line 5, page 7 to line 6 page 8:

“**2.2 Microphysical data and bulk scattering properties of the ice particle model**

In this study, microphysical data obtained in 11 field campaigns is used to generate the PSD of ice cloud particle using Eq. (3). To insure the unambiguously ice, microphysical data was filtered by limitation of the cloud temperature T≤-40°C. More than 14,000 individual PSD were selected to build bulk scattering properties of the ice particle models. The microphysical data is obtained from Space Science and Engineering Center, University of Wisconsin-Medison (http://www.ssec.wisc.edu/ice_models/microphysical_data.html).

$$n(D) = N_0 D^{\mu} e^{-\lambda D} \quad (3)$$

where D is the particle maximum dimension, $n(D)$ is the particle concentration per unit volume, N_0 is the intercept, λ is the slope, and μ is the dispersion.

Furthermore, spectral bulk scattering properties are calculated from SGLI single scattering database and derived PSD for used in the SAD analysis. Main steps for calculating the bulk scattering properties are as follows:

1) Extract the total projected area, total volume, maximum dimension, scattering cross section and scattering phase function parameters at a specific wavelength for 5 ice particle models from SGLI single scattering property database.
2) Calculate the effective diameter (D_{eff}) for 5 ice particle models based on the Eq. (4). The D_{eff} is

defined as a ratio of the total volume to the total projected area for a given PSD.

3) Calculate the scattering albedo ($\overline{A_s}$), asymmetry factor ($\bar{g}$) extinction efficiency ($\overline{Q_e}$) and scattering phase function ($\overline{P}$) for 5 ice particle models based on the Eq. (5), Eq. (6) Eq. (7) and Eq. (8).
4) Pick up the scattering albedo, asymmetry factor, extinction efficiency and scattering phase function with small, medium and large size of effective diameters, and average the selected parameters to obtain bulk scattering properties to be used in the SAD analysis.

$$D_{eff} = \frac{3}{2}\frac{\int_{D_{min}}^{Dmax} V(D)n(D)dD}{\int_{D_{min}}^{Dmax} A(D)n(D)dD} = \frac{3}{2}\frac{V_{Tot}}{A_{Tot}} \quad (4)$$

$$\overline{A_s} = \frac{\int_{D_{min}}^{Dmax} A_s\, n(D)dD}{\int_{D_{min}}^{Dmax} n(D)\, dD} \quad (5)$$

$$\bar{g} = \frac{\int_{D_{min}}^{Dmax} g(D,\lambda)\sigma_{sca}(D,\lambda)n(D)dD}{\int_{D_{min}}^{Dmax} \sigma_{sca}(D,\lambda)n(D)dD} \quad (6)$$

$$\bar{Q}_e = \frac{\int_{D_{min}}^{Dmax} \sigma_{ext}(D)A(D)n(D)dD}{\int_{D_{min}}^{Dmax} A(D)n(D)dD} \quad (7)$$

$$\bar{P}(\theta) = \frac{\int_{D_{min}}^{Dmax} P(\theta,D,\lambda)\sigma_{sca}(D,\lambda)n(D)dD}{\int_{D_{min}}^{Dmax} \sigma_{sca}(D,\lambda)n(D)dD} \quad (8)$$

where, D_{min} and D_{max} are minimum and maximum size of the ice particles, V_{Tot} and A_{Tot} are the total volumes and projected areas of the ice particles, respectively, A_s, g, σ_{sca}, σ_{ext} and P are the scattering albedo asymmetry factor, scattering cross section, extinction cross section and phase function for single particle, respectively, θ is the scattering angle."

Response to the comments of reviewer#2

In the big picture, this is the sort of study that should be done more often. The authors make a good faith effort to compare the ice cloud bulk scattering models currently developed by different groups in the scientific community for use with a variety of satellite (and other) programs and make the case for how the GCOM-C team is choosing its own ice cloud bulk scattering model. There is some interesting material in this article, but a close reading of the text also led to a number of questions that need to be addressed before publication. To me, it seems that the paper was submitted a bit too quickly as there are some loose ends that need to be tied up. The scientific issues will be listed below. I would also urge the authors to submit their revised paper to someone, perhaps a co-author or colleague, who will carefully edit it to improve the grammar. Further, the verb tenses need to be more consistent throughout the manuscript. The authors tend to jump between present and past tense. Because of the numerous grammatical changes I found in reading this manuscript, I will not attempt to list them and will confine my comments to the scientific questions.

1） Section 2, page 7, a lot of questions on my part: I am puzzled by the choice of habits chosen for comparison with the Voronoi particle for this study: hexagonal column, plates, bullet rosettes, and droxtals. In a given particle size distribution, is there any thought given to whether the choice of habits makes sense from a microphysical point of view, or was a habit chosen simply to provide a sense of different optical properties?

For example, droxtals were employed in the Collection 5 MODIS models to represent only the very smallest particles in a given size distribution. This habit was never meant to be used for any particle larger than a few tens of microns in size. In this study, droxtals of all sizes seem to be employed - why did the authors choose this habit for comparison? It should also be stated that for Collection 6, MODIS now uses only an aggregate of solid columns for its operational retrievals, not a habit mixture.

Answer: In this study, the hexagonal column, plates, bullet rosettes, and droxtal habits were chosen simply to provide a sense of different optical properties. The reason for adopting the droxtal habits with large sizes in the SAD analysis is not only for investigating the shape of the droxtal, but also for investigating whether the optical property of the Droxtal habits with varying size can satisfy the SAD measurements. Comparing with previous studies, we have more data processed and in a fully consistent manner so it does make sense in my view to keep the results for the other pristine models, although we will be emphasizing the results obtained for the Voronoi.

2) With regard to the choice of plates: plates do not tend to grow to sizes larger than about 500 microns and are not generally employed in bulk scattering models to represent large particles. What is the reasoning for using this habit at larger sizes?

Answer: Similar to the above answer, we employed the large particle (D_{eff} = 100 um) of the plate in this study to provide a sense of different optical properties and to further investigate the optimal particle model for ice cloud remote sensing.

3) With regard to the columns: are these hollow or solid? That is, are there hollow cavities at each end of the particle, or air bubbles within the particle?

Answer: The simple solid column models do not include air bubbles, were employed in this study. In the revised paper, we now use the term “solid” hexagonal ice column to avoid any confusion.

4) With regard to the bullet rosette: exactly what form of the bullet rosette did you use for your calculations? How many branches? Were the branches solid or did they have hollow cavities at the end of each branch?

Answer: As described in Line 3-4 Page 6, the definition of bullet rosettes in this study is same as the definition used in the scattering database by Yang et al., (2000).

Line 3, 4 Page 6: "The habits shown in Fig. 1 are defined with the same parameters (semi-width, length, aspect ratio and maximum dimension) as employed in the scattering properties database by Yang et al., (2000, 2005)."

5) I also have a number of questions about the Voronoi particle - this is a very interesting habit but little information is provided about it. Among the questions I have about this particle are the following:
(1) is a single particle adopted for each maximum diameter, or is a distribution of particles assumed from which an effective radius is calculated? This is not discussed.

Answer: Thank you very much for your valuable comments. The effective particle radius is defined as the radius of the volume-equivalent sphere (See Line 18-20, Page 6).

(2) I would like to see a figure that shows the total volume and total projected area as a function of particle size for the Voronoi particle, and for comparison show a more well-known particle such as the column. further, it would be interesting to see asymmetry parameter, single-scattering albedo (at a slightly absorbing wavelength) and maybe extinction efficiency as a function of effective radius/diameter.

Answer: According to the suggestion, we have plotted the variations of the total volume, total projected area, asymmetry parameter and single scattering albedo (at a slightly absorbing wavelength) for Voronoi and well-known particles of column and plate at 2.2um as shown in following Figure. We also added the variations of the single scattering albedo at wavelength of 1.05 and 2.21 micron in the modified manuscript (Fig. 4).

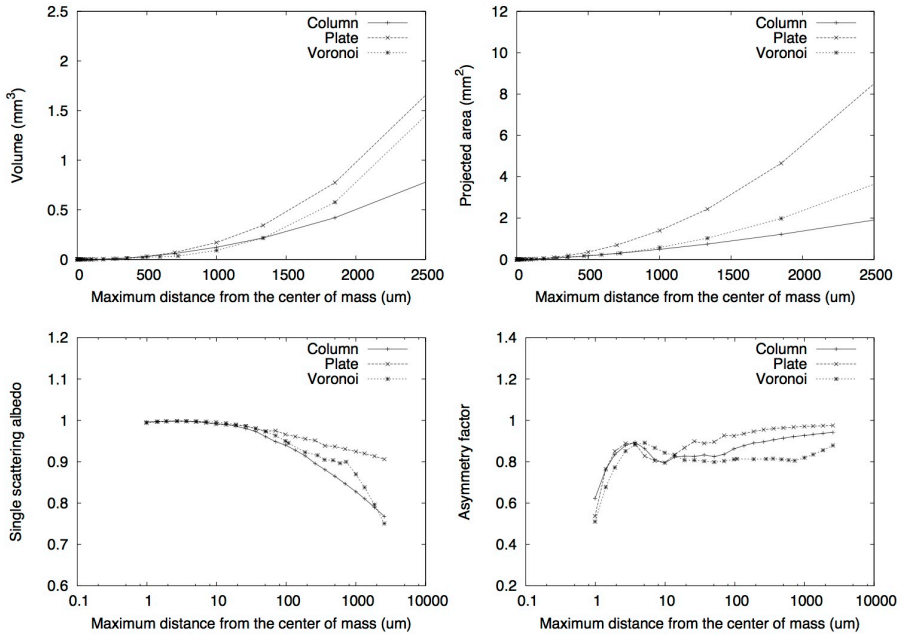

[Figure 1: Variations of volume, projected area, single scattering albedo and asymmetry factor as function of the maximum distance from the center of mass (half of the maximum dimension) for Voronoi, plate and column particles at a wavelength of 2.2um]

(3) if the Voronoi particle is used to represent all sizes, from the smallest to the very largest particles in a size distribution, what does it look like for very small particles? It would be illustrative to show a representation of this habit for very small, medium, and large sizes.

Answer: Figure 2 shows the various size of Voronoi models used in this study. Particle shapes as a function of maximum dimension are determined by in-situ observation of the ice particle images as illustrated by Baum et al., 2011. Detail of the Voronoi model is descripted by Ishimoto et al. (2012).

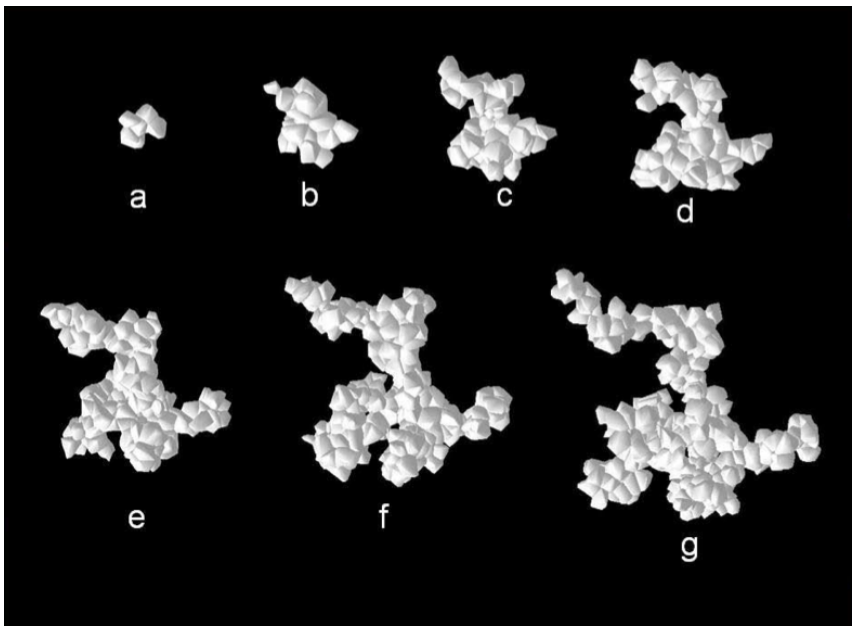

Figure 2: Various size and habit of Voronoi models (Ishimoto et al., 2012) (shape (a): size parameter (SZP) < 660; shape (b) – (g): 660 < SZP < 2250)

6) Section 3, questions regarding the use of SAD analysis: The authors are making heavy use of the SAD approach, and POLDER/PARASOL data, in their analysis for the optimal choice of ice habits/models for use by GCOM-C. As noted by the authors, the assumption in the SAD is that the ice clouds under analysis have a high optical thickness, generally having values greater than 5. So here are some questions relating to this:
(1.) Right away, this means that cirrus clouds are excluded as this subset of ice clouds generally has a much lower optical thickness. So I would suggest replacing "cirrus clouds" with "ice clouds" throughout the manuscript.

Answer: According to the suggestion, we have replaced "cirrus clouds" with "ice clouds" in the revised manuscript.

(2.) as a suggestion, use of the CALIPSO/CALIOP polarization lidar data would help to provide insight for optically thin ice clouds. It would be interesting to see how the Voroni particle behaves at low optical thickness values in direct comparison with the CALIOP retrievals. This could be done in future work, but it should be mentioned.

Answer: The suggestion by the reviewer is very important for further investigating the impact of the Voronoi particle on cirrus cloud retrievals. According to the suggestion, we have added the description about the suggested issue in the "conclusions" section of the revised manuscript as future work (Line 32-33, page 13).

(3.) Are there other factors that could be influencing the SAD analysis that could lead to less agreement in the icebox region for example? Or can we assume that the choice of habit is the key factor here?

Answer : Yes. Except for the particle habit, the surface roughness and whether the air bubbles included in the particles also influence the SAD analysis. For investigating the applicability of the Voronoi model, we compared it to the conventional ice particle models with surface roughness and air bubbles as shown in Figure 9 (please see the description in line 12-16, page 12).

In line 12-16, page 12: "As shown in Fig. 9, none of the selected models have strong angular dependencies. However, all the models in Fig. 9 have a rough surface, except for the IHM containing spherical air bubbles and Voronoi habit. This implies that the Voronoi habit model has a similar effect as some aggregated and mixed-habit ice particle models with roughened surfaces and the IHM single-particle model containing air bubbles on retrieval of the ice cloud properties using remote sensing instruments."

7) Section 4.1, page 12: The authors noted that the ice models currently in use now adopt particle roughening so that the solar-wavelength phase functions no longer have halos. Yet in Figure 4, results are shown for smooth ice particle habits in comparison with the Voronoi. The results in this figure should be changed so that all particles adopt roughening. Roughening is employed in other results, and the same assumption should be adopted with this figure too.

Answer: In the previous study, it was reported that some complex aggregate ice habit models, column particle including air bubbles and particle model with rough surface showed good agreement with the SAD analysis. However, it is difficult to say that the research of the single ice particle model with smooth surface has been investigated enough. In this study, we adopted the four smooth ice particle habits (column, plate, droxtal, bullet rosette) with various sizes for comparison with the Voronoi as shown in Figure 5.

8) Page 13, Figure 6: why show results at a wavelength of 1.05 microns rather than at 0.67 or 0.87 microns?

Answer: Normally, the wavelengths of 0.68μm and 0.86μm are useful for retrieving the cloud optical thickness. However, the 0.68μm and 0.86μm channels of the SGLI were designed to observe the vegetation, ocean color and aerosol in GCOM-C satellite program. The maximum radiance (MRad) in these channels is lower than that of the cloud observing channels. Thus, observed radiance in these channels easily saturate when observing thick cloud.

The wavelength of 1.05μm in the SGLI is designed to observe the cloud in GCOM-C mission. From Figure 6 we can also confirm that this channel is efficient for retrieving cloud properties.

9) Conclusions, page 17, line 10: as noted earlier, the use of the droxtal habit really does not make much sense. But my question for this conclusion is whether the results are based on smooth or roughened particles, or whether these particle model scattering properties are based on size distributions or simply a single particle for each given size - it's not clear to me.

Answer: As we stated in answer 1), the reason for using all sizes of the droxtal model is to provide a sense of different optical properties and to further investigate the optimal ice particle habit for retrieval of ice cloud properties.

Investigation of ice particle habits to be used for ice cloud remote sensing for the GCOM-C satellite mission

Husi LETU[1], Hiroshi ISHIMOTO[2], Jerome RIEDI[3], Takashi Y. NAKAJIMA[1], Laurent C.-LABONNOTE[3], Anthony J. BARAN[4], Takashi M. NAGAO[5], Miho SEKIGUCHI[6]

[1]Research and Information Center (TRIC), Tokai University, 4-1-1 Kitakaname Hiratsuka, Kanagawa 259-1292, Japan
[2]Meteorological Research Institute, 1-1 Nagamine, Tsukuba, Ibaraki 305-0052, Japan
[3]Laboratoire d'Optique Atmosphérique, UMR CNRS 8518, Université de Lille 1-Sciences et Technologies, Villeneuve d'Ascq, France
[4] Met Office, Fitzroy Road, Exeter, EX1 3PB, UK
[5] Earth Observation Research Center (EORC), Japan Aerospace Exploration Agency (JAXA), 2-1-1 Sengen Tsukuba, Ibaraki 305-8505, Japan
[6] Tokyo University of Marine Science and Technology, Tokyo 135-8533, Japan

(Corresponding author: Takashi Y. Nakajima Email: nkjm@yoyogi.ycc.u-tokai.ac.jp)

1 Introduction

Ice clouds play an important role in the radiation balance of the Earth's atmospheric system through interaction with solar radiation and infrared emissions (Liou, 1986; Baran, 2012). However, there are still large uncertainties in characterizing the microphysical and optical properties of ice clouds. This is because they consist of ice particles with a wide range of habits and sizes (C.-Labonnote et al., 2000; Forster et al., 2007; Baran et al., 2009; Cole et al., 2014; Yang et al., 2015). Different ice particle habits have varying single-scattering characteristics, resulting in different radiative properties. The only feasible way of inferring ice cloud properties on a global scale is to use satellite observations. In practice, one chooses an ice model, which may consist of a single habit or a mixture of habits, and look-up tables (LUTs) for ice cloud reflection and transmission characteristics are computed for a range of input optical properties such as optical thickness, cloud temperature, and effective particle size. The LUTs and a fast radiative transfer model are subsequentlyπ used for global operational retrievals. Thus, the choice of an ice model for a given satellite mission deserves rigorous investigation. The present study aims at better understanding the performance of several ice cloud habit models, in conjunction with applications to the Global Change Observation Mission-Climate (GCOM-C) satellite mission.

Over the past two decades, aircraft and balloon in situ observations and space-borne and ground-based remote sensing techniques have contributed greatly to understanding ice cloud microphysical and radiative properties (Baran et al., 1998; Baran et al., 1999; Baran et al., 2003; Heymsfield et al., 2002; Heymsfield, 2003; Zhang et al., 2009). A variety of ice particle models has been developed based on in situ observations, and single-scattering properties continue to draw a great deal of interest, particularly from the perspective of numerical computation (e.g., Macke et al., 1996a, 1996b; McFarquhar and Heymsfield, 1996; Yang et al., 2000, 2005, 2013; Um and McFarquhar, 2007, 2009, 2011; Nousiainen et al., 2011; Baum et al., 2005, 2011; Baran and C.-Labonnote, 2007; Ishimoto et al., 2012b; Liu et al., 2014). Light-scattering computation methods include the finite-difference time-domain (FDTD) method (Yee, 1966; Yang and Liou, 1998a; Sun et al., 1999, Ishimoto et al., 2012a), T-matrix (Havemann and Baran, 2001; Bi and Yang, 2014), the discrete dipole approximation method (Purcell and Pennypacker, 1973; Draine and Flatau, 1994; Yurkin et al., 2007), the pseudo-spectral time-domain method (Liu et al., 1997, 1998; Chen et al., 2008; Liu et al., 2012), the surface-integral equation method (Nakajima et al., 2009), the improved geometric optics method (IGOM) (Yang and Liou, 1996), and the

ray-tracing geometric optics method (GOM) (Takano, 1989, 1993; Macke, 1993; Macke et al. 1996a; Yang and Liou, 1998b; Masuda et al., 2012).

Based on one or more of these scattering models, single-scattering property libraries have been developed for certain habits. Hess et al. (1994) developed a single-scattering properties database for hexagonal plates and columns with a random orientation at wavelengths between 0.35 and 3.7 μm. Yang et al. (2000) developed a scattering and absorption property database for various ice particle habits with random orientation using the FDTD and IGOM methods at wavelengths between 0.2 and 5 μm. Six ice particle habits were selected in the calculations: plates, solid and hollow columns, planar bullet-rosettes, spatial bullet-rosettes, and aggregates. Yang et al. (2005) published a database for ice particles with eight different habits at 49 wavelengths between 3 and 100 μm, using a combination of several methods, including the FDTD, T-matrix, IGOM, and Lorenz–Mie theory. Recently, Yang et al. (2013) released a full set of scattering, absorption, and polarization properties assuming random orientation for a set of 11 habits at a number of wavelengths, ranging between 0.2 and 100 μm. The habits include droxtals, prolate spheroids, oblate spheroids, solid and hollow columns, and compact ice aggregates composed of eight solid hexagonal ice columns (hereafter, "8-column aggregate"), hexagonal plates, small spatial aggregates composed of 5 plates (hereafter, "5-plate aggregate"), large spatial aggregates composed of 10 plates, and solid and hollow bullet-rosettes. This library is based on the Amsterdam discrete dipole approximation, T-matrix, and IGOM methods. On the basis of this updated library, Baum et al. (2014) developed a new set of bulk scattering and absorption models with habit mixtures for use in ice cloud radiative transfer calculations and retrieval of ice cloud properties from remote sensing measurements. The ice crystal single-scattering databases of Baran and Francis (2004) and Baran et al. (2014) have been constructed from numerical simulations of individual ice crystals by using a combination of methods described in those papers.

This study is aimed at identifying an optimal choice of ice habits for the Global Change Observation Mission (GCOM-C) satellite. It is useful to provide a brief summary of what other teams have chosen for their operational products. Numerous articles have investigated the use of effective ice particle habits derived from various ice habit models and remote sensing measurements from multiple angles for use in cloud parameter retrievals (Baran et al., 1998; Chepfer, 1998; Baran et al., 1999; C.-Labonnote et al., 2000; Chepfer et al., 2001; Masuda et al., 2002; Baran et al., 2003; Knap et al., 2005; Sun et al., 2006;

Baran and Labonnote, 2006; Baran et al., 2007). C.-Labonnote et al. (2000, 2001) and Doutriaux et al. (2000) developed models of randomly oriented hexagonal ice particles containing spherical air bubbles (inhomogeneous hexagonal monocrystal (IHM) model) for use in the ice cloud retrievals of the POLarization and Directionality of the Earth's Reflectances (POLDER) measurements. Spherical albedo difference (SAD) analysis is employed to investigate the capability of the IHM model for retrieving the optical properties of ice clouds. It is illustrated that POLDER multi-angle measurements are sensitive to ice particle habit and roughness, at least for ice clouds having an optical thickness larger than 5. Chepfer et al. (2002) investigated effective ice particle habits using multi-angle and multi-satellite methods from visible reflectance satellite measurements. There is increasing evidence that the ice particle model should contain some degree of surface roughness (Foot, 1998; Baran et al., 2001; Baran et al., 2003; Ottaviani et al., 2012a; van Diedenhoven et al., 2012; Cole et al., 2013, 2014). Yi et al. (2013) reported that the general habit mixture model (GHM, Baum et al. 2011, 2014) provided significant differences in the shortwave cloud radiative effect in the National Center for Atmosphere Research Community Atmosphere Model (NCAR CAM 5). Baran and Labonnote (2007) developed an ensemble ice particle model for cirrus using various habits, including single hexagonal columns, a 6-branched bullet-rosette, and more complex 3-branched, 5-branched, 8-branched, and 10-branched particles. Baran et al. (2014) demonstrated that it is possible to simulate measured cirrus radiances from the UV to microwave frequencies by using the same micro-physically consistent habit mixture model throughout the spectrum. At solar wavelengths, Baran and Labonnote (2007) and Baran et al. (2014) showed that featureless phase functions best fit their multi-angle solar radiance measurements. Moreover, Baran et al. (2015) investigated the relation between the habit model of cirrus cloud particles and atmospheric relative humidity. These studies suggest that whatever ice model is employed, it should have a featureless phase function at solar wavelengths. Ishimoto et al. (2012b) developed a new habit of complex and highly irregular shapes called Voronoi aggregate, which is based on the ice particle images of convective ice clouds from in situ measurements. The phase function of the Voronoi habit varies smoothly with scattering angle, which is similar to behavior found from assuming severe surface roughness, including bubbles within the particle, or a combination of included bubbles and surface roughness. However, use of the Voronoi habit model for retrieval of the ice cloud optical thickness has not yet been investigated.

In this study, the single-scattering properties of the various ice particle models are calculated for developing the ice cloud property products of the GCOM-C Second Generation Global Imager (SGLI) satellite sensor. FDTD (Ishimoto et al., 2012a), geometric optics integral equation (GOIE) (Ishimoto et al., 2012a), and GOM (Masuda et al., 2012) methods are used to calculate the light-scattering properties of the Voronoi particle model, for a set of SGLI wavelengths. The SAD analysis is performed to investigate the optimal habit(s) using the POLDER-3 data. Furthermore, the results of the SAD analysis of the Voronoi habit model are compared with conventional GHM, the IHM model, and the 5-plate aggregate model of Yang et al. (2013).

2 Ice cloud models for the SGLI sensor

2.1 Single-scattering properties

Single-scattering properties for the five ice particle habits are calculated for the SGLI observation channels. The single-scattering properties are used to determine the optimal ice particle habits using the SAD method. The SGLI is the successor sensor to the Global Imager (GLI) onboard ADEOS-II, which takes measurements at wavelengths ranging from the near-ultraviolet to thermal infrared. The first satellite, GCOM-C1, is scheduled for launch in 2017 by the Japan Aerospace Exploration Agency (JAXA). The GCOM-C mission intends to establish a long-term satellite-observation system to measure essential geophysical parameters on the Earth's surface and in the atmosphere on a global scale, to facilitate the understanding of the global radiation budget, carbon cycle mechanism, and climate change (Imaoka et al., 2010). As shown in Table 1, SGLI has 19 channels, including two polarization channels at visible and near-infrared wavelengths. A detailed description of the SGLI is reported by Imaoka et al. (2010), Nakajima et al. (2011), and Letu et al. (2012).

Four of the ice particle habits (hexagonal columns, plates, bullet-rosettes, and droxtals) employed in this study were chosen by referring to MODIS collections-5 ice particle model (Baum et al., 2005) and ice cloud in-situ measurement data. The habits shown in Fig. 1 are defined with the same parameters (semi-width, length, aspect ratio and maximum dimension) as employed in the scattering properties database by Yang et al., (2000, 2005). The Voronoi habit is numerically determined by extraction of Wigner–Seitz cells from a 3-D mosaic image of the ice cloud microphysical data (Ishimoto et al., 2012b). This habit is different from the aggregate model used in the scattering database reported by Yang et al.

(1998b, 2013). Spatial Poisson–Voronoi tessellations are used to determine the complex structure of the ice particles for the 3-D mosaic image. The geometry of each cell in the Voronoi tessellation is defined and is based on the method by Ohser et al. (2000).

A combination of the FDTD, GOIE, and GOM methods is employed to calculate the single-scattering properties of Voronoi ice habits for a wide range of size parameters (SZP). The refractive index of ice published by Warren and Brandt (2008) is used in the computations. As shown in Table 2, the FDTD method is used to calculate the single-scattering properties of ice particles with small size parameters (SZP < 50). The GOIE and GOM methods are employed for calculating the scattering properties of ice particles with medium and large parameters, respectively. The wavelength selected for detailed calculations is determined by optimizing the results of the scattering database for the SGLI channels (Letu et al., 2010). Calculations are performed at 27 spectral wavelengths (λ) from the visible to the infrared spectral region in the SGLI channels shown in Table 2. The volume-equivalent radius (re) ranges from 0.7 to 533 μm, and is defined as a single particle radius of an equivalent volume sphere. The SZP ranges from 0.35 to 6098, and is given by

$$SZP = 2\pi \cdot re / \lambda \quad (1)$$

Consideration of the edge effect (Bi et al., 2010; Bi and Yang, 2014) is important for calculating the extinction efficiency (Q_{ext}) and absorption efficiency (Q_{abs}) by the GOIE method when the size parameter is less than 1000. The treatment of the edge effect is based on the method proposed by Ishimoto et al. (2012a). Correction coefficients are calculated from comparison results of the FDTD and GOIE as

$$Q_{ext} = Q_{ext/GOIE} + K_1 \cdot SZP^{-2/3}, \quad Q_{abs} = Q_{abs/GOIE} + K_2 \cdot SZP^{-2/3}, \quad (2)$$

where $Q_{ext/GOIE}$ and $Q_{abs/GOIE}$ are the extinction efficiencies calculated by the GOIE method. K_1 and K_2 are the coefficients of the edge-effect contribution. These coefficients are applied to correct the Q_{ext} and Q_{abs} of large particles calculated using GOIE, which is calculated by comparing Q_{ext} and Q_{abs} obtained from

FDTD and GOIE for maximum extension from the center of mass, ranging from 30 to 60 μm.

[Insert Fig. 1 about here]

[Insert Table 1 about here]

[Insert Table 2 about here]

2.2 Microphysical data and bulk scattering properties of the ice particle model

In this study, microphysical data obtained during eleven field campaigns is used to generate the PSDs of ice crystals using Eq. (3). To ensure the PSDs are unambiguously ice, microphysical data was filtered by limiting the cloud temperature to T≤-40°C. More than 14,000 individual PSDs were selected to build bulk scattering properties of the ice particle models. The microphysical data is obtained from Space Science and Engineering Center, University of Wisconsin-Medison (http://www.ssec.wisc.edu/ice_models/microphysical_data.html), and the PSDs are described by the following equation:

$$n(D) = N_0 D^{\mu} e^{-\lambda D} \quad (3)$$

where D is the particle maximum dimension, $n(D)$ is the particle concentration per unit volume, N_0 is the intercept, λ is the slope, and μ is the dispersion.

Furthermore, spectral bulk scattering properties are calculated from SGLI single-scattering database, and the derived PSDs are based on the method described in Baum et al., (2011). The main steps for calculating the bulk scattering properties are as follows:

5) Extract the total projected area, total volume, maximum dimension, scattering cross section and scattering phase function parameters at a specific wavelength for 5 ice particle models from the SGLI single scattering property database.
6) Calculate the effective diameter (D_{eff}) for 5 ice particle models based on Eq. (4).
7) Calculate the bulk-averaged single scattering albedo ($\overline{A_s}$), asymmetry factor ($\overline{g}$) extinction efficiency ($\overline{Q}_e$) and scattering phase function ($\overline{P}$) for 5 ice particle models based on Eqs (5–8).
8) Select the single scattering albedo, asymmetry factor, extinction efficiency and scattering phase

function with small, medium and large D_{eff}'s , and average the selected parameters over the PSDs to obtain the bulk scattering properties to be used in the SAD analysis.

$$D_{eff} = \frac{3}{2}\frac{\int_{D_{min}}^{D_{max}} V(D)n(D)dD}{\int_{D_{min}}^{D_{max}} A(D)n(D)dD} = \frac{3}{2}\frac{V_{Tot}}{A_{Tot}}$$

(4)

$$\overline{A_s} = \frac{\int_{D_{min}}^{D_{max}} A_s\, n(D)dD}{\int_{D_{min}}^{D_{max}} n(D)\, dD}$$

(5)

$$\bar{g} = \frac{\int_{D_{min}}^{D_{max}} g(D,\lambda)\sigma_{sca}(D,\lambda)n(D)dD}{\int_{D_{min}}^{D_{max}} \sigma_{sca}(D,\lambda)n(D)dD}$$

(6)

$$\bar{Q}_e = \frac{\int_{D_{min}}^{D_{max}} \sigma_{ext}(D)A(D)n(D)dD}{\int_{D_{min}}^{D_{max}} A(D)n(D)dD}$$

(7)

$$\bar{P}(\theta) = \frac{\int_{D_{min}}^{D_{max}} P(\theta,D,\lambda)\sigma_{sca}(D,\lambda)n(D)dD}{\int_{D_{min}}^{D_{max}} \sigma_{sca}(D,\lambda)n(D)dD}$$

(8)

where, D_{min} and D_{max} are the minimum and the maximum size of the ice particles, V_{Tot} and A_{Tot} are the total volumes and projected areas of the ice particles, respectively. The parameters A_s, g, σ_{sca}, σ_{ext} and P are the single scattering albedo, asymmetry factor, scattering cross-section, extinction cross-section, and phase function, respectively, for a single particle, and θ is the scattering angle.

3 Data and methods

Since 1996, three POLDER instruments have been flown to study clouds and aerosols with multiple angles and polarization capabilities. The POLDER-1 and POLDER-2 instruments aboard JAXA's ADEOS satellite were operated from November 1996 to June 1997 and December 2002 to October 2003, respectively. Both of the POLDER instruments observed intensity from 14 viewing directions with scattering angles from 60° to 180°. The spatial resolution of the product derived from POLDER-2 observation data is approximately 20 km, which is composed of 3 × 3 single pixels. POLDER-2 can

measure the upwelling total and polarized radiances from eight observing channels centered at wavelengths of 0.443, 0.490, 0.565, 0.670, 0.763, 0.765, 0.865, and 0.910 μm (Baran et al., 2006). POLDER-3 aboard the Polarization and Anisotropy of Reflectances for Atmospheric Sciences coupled with Observations from a lidar microsatellite (PARASOL), launched in 2004. The POLDER-3 has nine observing channels, three of which have polarization capabilities. PARASOL/POLDER-3 views a given scene at up to 16 angles as the satellite passes overhead. However, the capabilities of the instrument, such as observing the radiances from multiple viewing angles in several visible channels, are important for investigating the representative ice particle models for retrieving ice cloud properties. In this study, 589 × 246 pixels of the POLDER-3 observation data with a global scale over ocean from days 20–22 of March, June, September, and December 2008 are used to retrieve cloud optical thickness and spherical albedo for investigating the behavior of the five ice particle habits.

Figure 2(a) shows the distribution of the number of directional samples used in the SAD analysis. The number of pixels is increased in the scattering angle range of 60° to 160° and is decreased in the scattering angle range from 160° to 180°. There is a changing peak of the number of sample pixels in the scattering angle range of 140° to 160°. Figure 2(b) indicates the variation of the number of pixels by latitude; the number of pixels changes significantly as a function of latitude and is lowest when the latitude is around 90°N and 90°S. C.-Labonnote et al. (2000) and Baran et al. (2006) proposed the SAD method for testing the phase function of the various ice particle models using POLDER observational data with multiple viewing angles. For investigating the phase functions (P_{11}) of the different ice crystal models for retrieving the cloud microphysical properties, the cloud spherical albedo as a function of scattering angle is required. For calculating the cloud spherical albedo, bi-directional reflection is first determined by

$$R_{cld}(\mu, \mu_0, \phi - \phi_0) = \pi L_{obs}(\mu, \mu_0, \phi - \phi_0)/\mu_0 F_0 , \quad (9)$$

where u, and u_0 are cosines of the satellite and solar zenith angles, $\phi - \phi_0$ is the relative azimuth angle between the satellite and the sun, L_{obs} is the reflected solar radiance observed by the satellite, and F_0 is the

solar flux density. Cloud-plane albedo (A_p) and spherical albedo (S) are calculated by integrating over all the zenith and azimuth angles as

$$A_p(\mu_0) = \iint R_{cld}(\mu, \mu_0, \phi - \phi_0)\mu d\mu d\phi, \quad (10)$$

$$S = \int A_p(\mu_0)\mu_0 d\mu_0, \quad (11)$$

The value of cloud spherical albedo ($S(\theta)$) can be calculated from the L_{obs} in each pixel of the POLDER measurements with various scattering angles (θ) to investigate the P_{11} element of the ice particle models. The total observation number (N) of L_{obs} with various θ values is up to 16, and is limited to the viewing geometries of the measurements. Baran et al. (2006) assumed that if the scattering phase function of the ice particle model is correct, then calculated $S(\theta)$ in each direction should be the same and the SAD, as shown in Eq. (13), should be 0. $\bar{S}$, SAD, and θ are given as

$$\bar{S} = (1/N)\sum S(\theta) \quad (12)$$

$$SAD = S(\theta) - \bar{S} \quad (13)$$

$$cos\ \theta\ = cos(\pi - u_0)cos\ u\ +\ sin\ u_0\ sin\ u \cos(\phi - \phi_0), \quad (14)$$

where u_0 and u are the solar and satellite zenith angles, respectively.

The steps for applying the SAD analysis to POLDER-3 measurements are as follows:

9) Calculate spherical albedo from the POLDER-3 measurements with 16 viewing geometries for each of the ice particle models.
10) Perform the SAD analysis by taking the difference between the directional and the direction-averaged cloud spherical albedo.
11) Assume that the phase function for each ice particle model adequately represents the phase function for all ice particles in each pixel of the satellite measurement, and that the retrievals of the optical thickness and spherical albedo from the POLDER measurements with different viewing geometries are the same.

When SAD is 0, the mean spherical albedo and the spherical albedo from the specific angle of POLDER-3 measurements are the same. Therefore, the criteria for selecting the optimal particle habit of the ice cloud are defined as a SAD near 0 in the 16 viewing geometries of POLDER-3 and a small angular dependence.

[Insert Fig. 2 about here]

4 Results and discussion

4.1 Characteristics of the scattering properties

To confirm the accuracy of the calculated single-scattering properties, the phase functions computed in this study are compared with other results. Figure 3 shows comparisons of the phase function (P_{11}) of hexagonal and spheroid particles calculated from the FDTD method with those derived from the ADDA (Bi et al., 2011) and T-Matrix methods, respectively. Our FDTD results are the same as those calculated with the other methods. In addition, Ishimoto et al. (2012b) and Masuda et al. (2012) verify that the phase functions of ice particles with medium and large size parameters are the same by comparing the GOIE and GOM results, respectively.

The single-scattering albedo, asymmetry factor and extinction efficiency are some of the key parameters of the single-scattering properties of ice particles. Figure 4 shows the single-scattering properties of various ice particle habits at wavelengths of 1.05 and 2.2 μm for various size parameters. The value of single-scattering albedo is close to 1.0 when size parameters are less than approximately 200 and 50 at wavelength 1.05 and 2.21, respectively; and the value decreases when size parameter is increasing. There is a smooth peak in the asymmetry factor for size parameters of 1 to 10, and the peak of the asymmetry factor at a wavelength of 2.1 μm is larger than that at 1.05 μm. The extinction efficiency increases with the size parameter up to approximately 10 and converges gradually to 2 when the size parameter exceeds 100. The maximum values of the extinction efficiency appear when the size parameter is around 10. However, the location of the maximum extinction efficiency varies with particle habit.

Bulk scattering phase functions of the column, droxtal, plate, bullet-rosette, and Voronoi habit with various effective diameters at wavelengths of 1.05 um are given in Figure 5. The phase functions depend on the particle habit and effective diameters. There is a halo peak for the column, plate and bullet-rosette

habit when effective diameters are 60 um and 100 um, as particle roughening is not applied in these calculations. For the droxtal, variation of the phase function is evident for different effective diameters. The POLDER-3 measures intensity from 16 viewing directions at scattering angles between 60˚–180°; for these scattering angles, the phase function curves of the various particles are different. The phase function of the Voronoi habit is very smooth, with features similar to those for severely roughened ice particle models and the IHM model except for the halo peak region as reported by Yang et al. (2013) and Doutriaux et al. (2000).

[Insert Fig. 3 about here]

[Insert Fig. 4 about here]

[Insert Fig. 5 about here]

4.2 SAD analysis

Figure 6 shows the SAD analysis as a function of the scattering angle, effective particle radius, and ice particle model. The SAD of the droxtal, column and plate show substantial variations in both the scattering angle and effective particle radius. The variation of SAD for the bullet-rosette model is more smoothly distributed close to 0 value of the SAD (hereafter, "zero line") than with the droxtal, plate, and column models for small (D_{eff} = 10 μm), medium (D_{eff} = 60 μm), and large particles (D_{eff} = 100 μm). However, the SAD peak of the bullet-rosette model varies in the scattering angle range of 140° to 160° with medium and large particles. The SAD of the Voronoi model is closest to the zero line over the entire scattering angle range for small, medium and large particles. Both the Voronoi and bullet-rosette model with small particles are smoothly distributed along the zero line.

Figure 7 shows the slope of the regression function (SRF) and total relative albedo difference (TRAD) of the SAD for the same five ice particle models with small, medium and large particles as shown in Fig.6. Both values of the SRF and TRAD for small particles of the bullet-rosette, for medium and large particles of the bullet-rosette and Voronoi models, are smallest of all the single particle models considered. However, there is a changing peak of the SAD in the scattering angle range of 140° to 160° for bullet-rosette model with medium and large particles. The SRF and TRAD for all size of particles with

droxtal model are largest in the all ice particle models. As we have described in section 3, the optimal particle habit is defined as a smallest value of the SRF and TRAD. Thus, it was confirmed that the bullet-rosette model with small particles and Voronoi model with medium and large particles are sufficiently accurate for the retrieval of the ice cloud spherical albedo and optical thickness. Thus, these models are sufficient to represent ice cloud in terms of optimal particle habit for the purposes of the SGLI sensor.

Ice crystals in ice cloud are complex. To simulate this complexity, we assume different values of distortion (as defined by Macke et al 1996) and apply these to the ensemble model. Numerous previous studies have shown that the degree of distortion is an important property to consider when retrieving ice cloud optical properties from multiple-view instruments. To investigate the influence of the distortion of the ice particle model on retrieval of the ice cloud property, we performed the SAD analysis using the ensemble ice particle models with D_{eff} = 60 μm, assuming a number of distortion values (see Fig. 8). The variation of SAD for the no distortion model in Fig. 8 (a) is largest relative to the other distortion values. As a function of distortion value, there are significant variations in the SAD analysis in the scattering angle range of 60° to 80° and 140° to 160°. There is no obvious difference of the SAD between Fig. 8 (b), Fig. 8 (c) and Fig. 8 (d) for various degrees of the distortions. The SAD of the ice particle models with a distortion values of 0.4 with spherical air bubbles in Fig. 8 (e) is closest to the zero line. It is implied that the models with distortion or surface roughness are best for the retrieval of the ice cloud optical property than with no distortion applied to the model. The model with spherical air bubbles and distortion is most efficient than the models with distortion only.

Several conventional studies demonstrated that ice particle models such as the ensemble ice particle model, IHM and GHM, and some aggregated complex models with rough surfaces are useful for operational satellite data processing (C.-Labonnote et al. 2000, 2001; Doutriaux et al. 2000; Baum et al. 2011, 2014; Baran and Labnnote, 2006, 2007; Cole al. 2013). For evaluating the accuracy of the Voronoi model, the SAD of the Voronoi model is compared with that of the conventional IHM, GHM, 5-plate aggregate, and ensemble ice particle models with D_{eff} = 60 μm. As shown in Fig. 9, none of the selected models have strong angular dependencies. However, all the models in Fig. 9 have a rough surface, except for the IHM containing spherical air bubbles and Voronoi habit. This implies that the Voronoi habit

model has a similar effect as some aggregated and mixed-habit ice particle models with roughened surfaces and the IHM single-particle model containing air bubbles on retrieval of the ice cloud properties using remote sensing instruments.

Figure 10 shows the slope of the regression function (top panel) and total relative albedo difference (bottom panel) for the selected models in Fig. 9. The SRF for the GHM, Voronoi, and averaged-ensemble models is significantly smaller than the other three models. The TRAD values for each habit model are not significantly different. However, that for the Voronoi model is slightly smaller than for the other models, except for the ensemble ice particle models. The Voronoi and ensemble-averaged models have small values of SRF and TRAD, indicating that the SAD of the Voronoi and averaged-ensemble model have a low angular dependence.

[Insert Fig. 6 about here]

[Insert Fig. 7 about here]

[Insert Fig. 8 about here]

[Insert Fig. 9 about here]

[Insert Fig. 10 about here]

5 Conclusions

Ice particle single-scattering properties are investigated for potential use in the GCOM-C satellite program. The single-scattering properties of five different ice particle models (plates, columns, droxtals, bullet-rosettes, and Voronoi) are developed using the FDTD, GOIE and GOM methods. The accuracy of the single-scattering property is investigated by comparing the phase function from the FDTD method used in this study to conventional results from ADDA and T-Matrix method. The FDTD phase functions are also compared with computational results from GOIE. Results indicate that the FDTD-based phase functions are consistent with results from the ADDA, T-Matrix and GOIE methods and suggest that the single-scattering property database developed in this study is reliable for use in radiative transfer simulations and applications in the remote sensing of ice cloud.

The characteristics of the single-scattering property database for five different ice particle models are investigated by analyzing the single scattering albedo, asymmetry factor and extinction efficiency. Bulk scattering phase function for five different ice particle models at wavelengths of 1.05 um is compared as a function of various effective diameters. It is concluded that phase functions depend on the particle habit and effective diameters. There is a halo peak for a middle and large size of column, plate and bullet-rosette habit. For the droxtal particle, variation of the phase function is evident for different effective diameters. The phase function of the Voronoi habit is very smooth, with features similar to those for severely roughened ice particle models.

Furthermore, SAD analysis is performed to determine the optimal ice particle habit for retrieving the optical thickness and cloud spherical albedo using POLDER-3 multi-angle measurements. Retrievals are performed using 589 × 246 pixels of the POLDER-3 observation data with a global scale over ocean from days 20–22 of March, June, September, and December 2003. The following conclusions are drawn from the results.

1) The SADs of the droxtal and column habits show significant variations with scattering angle and effective particle radius.
2) SAD variation for small particles with the bullet-rosette model is more smoothly distributed along the zero line than that with other habit models.
3) Voronoi model SAD is closest to the zero line with scattering angle for all particle sizes.
4) The bullet-rosette habit for small particles and Voronoi habit for all particle sizes are most suitable for retrieving the ice cloud spherical albedo and optical thickness.

The results of SAD analysis from the Voronoi model are compared with results from the conventional IHM, GHM, 5-plate aggregate, and ensemble ice particle models with moderate ice particle size to evaluate the efficiency of the Voronoi model on retrieving ice cloud optical properties. It is concluded that the Voronoi habit model is similar to the conventional models for retrieval of ice cloud properties with thick optical thickness using remote sensing instruments. The results of this study should be useful not only for developing the ice cloud products of the GCOM-C/SGLI satellite mission, but also for determining the optimal ice particle habit for ice cloud remote sensing. In future work, we will investigate how the Voroni particle behaves at low optical thickness values in direct comparison with the retrievals from CALIPSO/CALIOP polarization lidar data.

Acknowledgments.

This work was supported by the GCOM-C/SGLI and EarthCARE project of the Japan Aerospace Exploration Agency (JAXA), and the Japan Science and Technology Agency (JST), CREST/EMS/TEEDDA. The authors would like to thanks ICARE and CNES for providing the POLDER data as well as François Thieuleux for his support with POLDER data analysis. The authors gratefully acknowledge Dr. Bryan A. Baum (UW-Madison) for providing the GHM ice particle model.

References

Baran, A. J., Watts, P. D., and Foot, J. S.: Potential retrieval of dominating crystal habit and size using radiance data from a dual-view and multiwavelength instrument: A tropical cirrus anvil case. J. Geophys. Res., 103(D6), 6075–6082, 1998.

Baran, A. J., Watts, P. D., and Francis, P. N.: Testing the coherence of cirrus microphysical and bulk properties retrieved from dual-viewing multispectral satellite radiance measurements. J. Geophys. Res., 104(D24), 31673–31683, 1999.

Baran A. J., Francis, P. N., Labonnote, L. C., Doutriaux-Boucher, M.: A scattering phase function for ice cloud: Tests of applicability using aircraft and satellite multi-angle multiwavelength radiance measurements of cirrus.Q. J. R. Meteorol. Soc. 127: 2395 – 2416, 2001.

Baran, A. J, Havemann, S, Francis, P. N, Watts, P. D.: A consistent set of single-scattering properties for cirrus cloud: tests using radiance measurements from a dual-viewing multi-wavelength satellite-based instrument. JQSRT, 79–80:549–67, 2003.

Baran, A. J. and C.-Labonnote, L.: On the reflection and polarization properties of ice cloud, J. Quant. Spectrosc. Ra., 100, 41–54, 2006.

Baran, A. J. and C.-Labonnote, L.: A ensemble ice particle scattering model for cirrus, I: The solar region, Q. J. Roy. Meteor. Soc., 133, 1899–1912, 2007.

Baran, A. J., Hill, P., Furtado, K., Field, P., and Manners, J.: A Coupled Cloud Physics–Radiation Parameterization of the Bulk Optical Properties of Cirrus and Its Impact on the Met Office Unified Model Global Atmosphere 5.0 Configuration, J. Climate, 27, 7725-7752, **2014**.

Baran, A. J., Furtado, K., Labonnote, L. C., Havemann, S., Thelen, J. C., and Marenco, F.: On the relationship between the scattering phase function of cirrus and the atmospheric state. Atmos. Chem. Phys., 15, 1105–1127, 2015.

Baum, B. A., Yang, P., Heymsfield, A. J., Platnick, S., King, M. D., and Bedka, S. T.: Bulk scattering models for the remote sensing of ice clouds. Part 2: Narrowband models, J. Appl. Meteorol., 44, 1896–1911, 2005.

Baum, B. A., Yang, P., Heymsfield, A. J., Schmitt, C., Xie, Y., Bansemer, A., Hu, Y.-X., and Zhang, Z.: Improvements to shortwave bulk scattering and absorption models for the remote sensing of ice clouds, J. Appl. Meteorol. Clim., 50, 1037–1056, 2011.

Baum, B. A., P. Yang, A. J. Heymsfield, A. Bansemer, B. H. Cole, A. Merrelli, C. Schmitt, and C. Wang.: Ice cloud single-scattering property models with the full phase matrix at wavelengths from 0.2 to 100 μm, J. Quant. Spectrosc. Radiat. Transfer, 146, 123-139, 2014.

Bi, L., P. Yang, G. W. Kattawar.: Edge-effect contribution to the extinction of light by dielectric disk and cylindrical particles, Appl, Opt, 49, 4641-4646, 2010.

Bi, L., Yang, P., Kattawar, G. W., Hu, Y., and Baum, B. A.: Scattering and absorption of light by ice particles: solution by a new physical-geometric optics hybrid method, J. Quant. Spectrosc. Radiat. Transfer., 112(9), 1492-1508, 2011.

Bi, L., and P. Yang.: High-frequency extinction efficiencies of spheroids: rigorous T-matrix solutions and semi-empirical approximations, Optics Express, 22, 10270-10293, 2014.

Bi, L., and P. Yang.: Accurate simulation of the optical properties of atmospheric ice crystals with invariant imbedding T-matrix method. J. Quant. Spectrosc. Radiat. Transfer, 138,17-35, 2014.

Chen G, Yang P, Kattawar GW.: Application of the pseudospectral time-domain method to the scattering of light by nonspherical particles, J Opt Soc Am A, 25, 785–90, 2008.

Chepfer, H., Brogniez, G., and Fouquart, Y.: Cirrus clouds' mi- crophysical properties deduced from POLDER observations, J. Quant. Spectrosc. Radiat. Transfer, 60, 375–390, 1998.

Chepfer, H., Goloub, P., Riedi, J., de Haan, J. F., and Hove- nier, J. W.: Ice crystal shapes in cirrus clouds derived from POLDER-1/ADEOS-1, J. Geophys. Res., 106, 7955–7966, doi:10.1029/2000JD900285, 2001.

Chepfer, H., P. Minnis, D. Young, L. Nguyen, and R. F. Arduini, Estimation of cirrus cloud effective ice crystal shapes using visible reflectances from dual-satellite measurements, J. Geophys. Res., 107(D23), 4730, doi:10.1029/2000JD000240, 2002.

Cole, B., P. Yang, B. A.Baum, J. Riedi, L. C.-Labonnote, F. Thieuleux, and S. Platnick.: Comparison of PARASOL observations with polarized reflectances simulated using different ice habit mixtures, J. Appl. Meteor. Clim. 52, 186-196, 2013.

Cole, B. H., P. Yang, B. A. Baum, J. Riedi, and L. C.-Labonnote.: Ice particle habit and surface roughness derived from PARASOL polarization measurements, Atmos. Chem. Phys., 14, 3739-3750, doi:10.5194/acp-14-3739-2014, 2014.

Doutriaux-Boucher, M., Buriez, J. C., Brogniez, G., Labonnote, L. C., and Baran, A. J.: Sensitivity of retrieved POLDER directional cloud optical thickness to various ice particle models. Geophys. Res. Lett., 27, 109–112, 2000.

Draine, B. T., and Flatau, P. J.: Discrete-dipole approximation for scattering calculations. JOSA A, 11(4), 1491-1499, 1994.

Foot, J. S.: Some observations of the optical properties of clouds. II: Cirrus. Q. J. R. Meteorol. Soc., 114, 145–164, 1988.

Forster, P., Ramaswamy, V., Artaxo, P., Berntsen, T., Betts, R., Fahey, D., Haywood, J., Lean, J., Lowe, D., Myhre, G., Nganga, J., Prinn, R., Raga, G., Schulz, M., and Van Dorland, R.: Changes in Atmospheric Constituents and in Radiative Forcing, in: IPCC Fourth Assessment Report WG 1, Solomon, S., Qin, D., Manning, M., Chen, Z., Marquis, M., Averyt, K. B., Tignor, M., and Miller, H. L. (Eds.), Cambridge University Press, Cambridge, UK, 129–234, 2007.

Hess, M., and M. Wiegner.: COP: A data library of optical properties of hexagonal ice crystals. Appl. Opt., 33, 7740–7746, 1994.

Heymsfield, A. J., Bansemer, A., Field, P. R., Durden, S. L., Stith, J. L., Dye, J. E., Hall, W., and Grainger, C. A.: Observations and Parameterizations of Particle Size Distributions in Deep Tropical Cirrus and Stratiform Precipitating Clouds: Results from In Situ Observations in TRMM Field Campaigns, J. Atmos. Sci., 59, 3457–3491, 2002.

Heymsfield, A. J.: Properties of Tropical and Midlatitude Ice cloud Particle Ensembles. Part I: Median Mass Diameters and Terminal Velocities, J. Atmos. Sci., 60, 2573–2591, 2003.

Imaoka, K., Kachi, M., Fujii, H., Murakami, H., Hori, M., Ono, A., and Shimoda, H.: Global Change Observation Mission (GCOM) for monitoring carbon, water cycles, and climate change. Proceedings of the IEEE, 98(5), 717-734, 2010.

Ishimoto, H., Masuda, K., Mano, Y., Orikasa, N., and Uchiyama, A.: Optical modeling of irregularly shaped ice particles in convective cirrus. In radiation processed in the atmosphere and ocean (IRS2012): Proceedings of the International Radiation Symposium (IRC/IAMAS) 1531, 184-187, 2012a.

Ishimoto, H., Masuda, K., Mano, Y., Orikasa, N., and Uchiyama, A.: Irregularly shaped ice aggregates in optical modeling of convectively generated ice clouds, J. Quant. Spectrosc. Radiat. Transfer, 113, 632–643, 2012b.

Knap, W. H., L. C.-Labonnote, G. Brogniez, and P. Stammes.: Modeling total and polarized reflectances of ice clouds: Evaluation by means of POLDER and ATSR-2 measure- ments. Appl. Opt., 44, 4060–4073, 2005.

C.-Labonnote, L., Brogniez, G., Doutriaux-Boucher, M., Buriez, J. C., Gayet, J. F., and Chepfer, H.: Modeling of light scattering in cirrus clouds with inhomogeneous hexagonal monocrystals. Comparison with in-situ and ADEOS-POLDER measurements, Geophys. Res. Lett., 27, 113–116, 2000.

C.-Labonnote, L., Brogniez, G., Buriez, J. C., and Doutriaux- Boucher, M.: Polarized light scattering by inhomogeneous hexagonal monocrystals: validation with ADEOS-POLDER measurements, J. Geophys. Res. 106, 12139–12153, 2001.

Letu, H., Nakajima, T. Y., and Matsui, T. N.: Development of an ice crystal scattering database for the global change observation mission/second generation global imager satellite mission: Investigating the refractive index grid system and potential retrieval error. Appl. Opt., 51, 6172-6178, 2012.

Liou, K. N.: Influence of Cirrus Clouds on Weather and Climate Processes: A Global Perspective, Mon. Weather Rev., 114, 1167–1199, 1986.

Liu, Q. H.: The PSTD algorithm: a time-domain method requiring only two cells per wavelength, Microwave Opt. Technol. Lett., 15, 158–165, 1997.

Liu, Q. H.: The pseudospectral time-domain (PSTD) algorithm for acoustic waves in absorptive media, IEEE Trans. Ultrason. Ferroelectr. Freq. Control, 45, 1044–1055, 1998.

Liu, C., Panetta, R. L., Yang, P.: Application of the pseudo-spectral time domain method to compute particle single-scattering properties for size parameters up to 200, J. Quant. Spectrosc. Radiat. Transfer., 113, 1728-1740, 2012.

Liu, C., Yang, P., Minnis, P., Loeb, N., Kato, S., Heymsfield, A., and Schmitt, C.: A two-habit model for the microphysical and optical properties of ice clouds, Atmos. Chem. Phys., 14, 13719-13737, 2014.

Macke, A.: Scattering of light by polyhedral ice crystals. Applied Optics., 32, 2780-2788, 1993.

Macke, A., Mishchenko, M. I., and Cairns, B.: The influence of inclusions on light scattering by large ice particles, J. Geophys. Res., 101, 23311–23316, 1996a.

Macke, A., Mueller, J., and Raschke, E.: Single Scattering Properties of Atmospheric Ice Crystals, J. Atmos. Sci., 53, 2813–2825, 1996b.

Masuda, K., Ishimoto, H., and Takashima, T.: Retrieval of cirrus optical thickness and ice-shape information using total and polarized reflectance from satellite measurements. J. Quant. Spectrosc. Radiat. Transfer, 75, 39-51, 2002.

Masuda, K., Ishimoto, H., and Mano, Y.: Efficient method of computing a geometric optics integral for light scattering, Meteorology and Geophysics ., 63, 15–19, 2012.

McFarquhar, G. M., and Heymsfield, A. J.: Microphysical characteristics of three anvils sampled during the Central Equatorial Pacific Experiment. J. Atmos. Sci., 53, 2401-2423, 1996.

Nakajima, T. Y., Nakajima, T., Yoshimori, K., Mishra, S. K., and Tripathi, S. N.: Development of a light scattering solver applicable to particles of arbitrary shape on the basis of the surface integral equations method of Muller-type (SIEM/M): Part I. Methodology, accuracy of calculation, and electromagnetic current on the particle surface, Appl. Opt., 48, 3526–3536, 2009.

Nakajima, T. Y., Tsuchiya, T., Ishida, H., Matsui, T. N., and Shimoda, H.; Cloud detection performance of spaceborne visible-to-infrared multispectral imagers. Applied optics, 50(17), 2601-2616, 2011.

Nousiainen, T., Lindqvist, H., McFarquhar, G. M., and Um, J.: Small irregular ice crystals in tropical cirrus, J. Atmos. Sci., 68, 2614–2627, doi:10.1175/2011JAS3733.1, 2011.

Ohser, J., Mu¨cklich F.: Statistical analysis of microstructures in materials science, Chichester: Wiley; 2000.

Ottaviani, M., Cairns, B., Chowdhary, J., van Diedenhoven, B., Knobelspiesse, K., Hostetler, C., Ferrare, R., Burton, S., Hair, J., Obland, M., and Rogers, R.: Polarimetric retrievals of surface and cirrus clouds properties in the region affected by the deep- water horizon oil spill, Remote Sens. Environ., 121, 389–403, doi:10.1016/j.rse.2012.02.016, 2012.

Purcell, E. M., and Pennypacker, C. R.: Scattering and absorption of light by nonspherical dielectric grains. The Astrophysical Journal, 186, 705-714, 1973.

Sun, W., Q. Fu, and Z. Chen.: Finite-difference time-domain solution of light scattering by dielectric particles with perfectly matched layer absorbing boundary conditions. Appl. Opt., 38, 3141–3151, 1999.

Sun, W., Loeb, N., and Yang, P.: On the retrieval of ice cloud particle shapes from POLDER measurements, J. Quant. Spectrosc. Radiat. Transfer., 2006.

Takano, Y. and Liou, K. N.: Solar radiative transfer in cirrus clouds. Part I. Single-scattering and optical properties of hexagonal ice crystals, J. Atmos. Sci., 46, 3–19, 1989.

Takano, Y., and Liou, K. N.: Transfer of polarized infrared radiation in optically anisotropic media: application to horizontally oriented ice crystals., JOSA A, 10, 1243-1256, 1993.

Um, J. and McFarquhar, G. M.: Single-scattering properties of aggregates of bullet rosettes in cirrus, J. Appl. Meteorol. Clim., 46, 757–775, doi:10.1175/JAM2501.1, 2007.

Um, J. and McFarquhar, G. M.: Single-scattering properties of aggregates of plates, Q. J. Roy. Meteorol. Soc, 135, 291–304, doi:10.1002/qj.378, 2009.
Um, J. and McFarquhar, G. M.: Dependence of the single-scattering properties of small ice crystals on idealized shape models, Atmos. Chem. Phys., 11, 3159–3171, doi:10.5194/acp-11-31592011, 2011.
Van Diedenhoven, B., Cairns, B., Geogdzhayev, I. V., Fridlind, A. M., Ackerman, A. S., Yang, P., and Baum, B. A.: Remote sensing of ice crystal asymmetry parameter using multi- directional polarization measurements – Part 1: Methodology and evaluation with simulated measurements, Atmos. Meas. Tech., 5, 2361–2374, doi:10.5194/amt-5-2361-2012, 2012.
Van Diedenhoven, B., A.M. Fridlind, B. Cairns, and A.S. Ackerman.: Variation of ice crystal size, shape and asymmetry parameter in tops of tropical deep convective clouds. J. Geophys. Res. Atmos., 119, no. 20, 11809-11825, 2014.
Warren, S. G., and Brandt, R. E.: Optical constants of ice from the ultraviolet to the microwave: A revised compilation. J. Geophys. Res, (1984–2012), 113(D14), 2008.
Yang, P., and Liou, K. N.: Geometric-optics—integral-equation method for light scattering by nonspherical ice crystals. Appl. Optics, 35, 6568-6584, 1996.
Yang, P., and K. N. Liou.: An efficient algorithm for truncating spatial domain in modeling light scattering by finite-difference technique, J. Comput. Phys., 140, 346-369, 1998a.
Yang, P. and Liou, K. N.: Single-scattering properties of complex ice crystals in terrestrial atmosphere, Contrib. Atmos. Phys., 71, 223–248, 1998b.
Yang, P., K. N. Liou, K. Wyser, and D. Mitchell.: Parameterization of the scattering and absorption properties of individual ice crystals., J. Geophys. Res., 105, 4699-4718, 2000.
Yang, P., H. Wei, H.-L. Huang, B. A. Baum, Y. X. Hu, G. W. Kattawar, M. I. Mishchenko, and Q. Fu.: Scattering and absorption property database for nonspherical ice particles in the near- through far-infrared spectral region., Appl. Opt. 44, 5512-5523, 2005.
Yang, P., L. Bi, B. A. Baum, K. N. Liou, G. W. Kattawar, M.I. Mishchenko, and B. Cole.: Spectrally consistent scattering, absorption, and polarization properties of atmospheric ice crystals at wavelengths from 02 to 100 μm. J. Atmos. Sci., 70, 330-347, 2013.
Yang, P., K. N. Liou, L. Bi, C. Liu, B. Q. Yi, and B. A. Baum.: On the radiative properties of ice clouds: Light scattering, remote sensing, and radiation parameterization. Adv. Atmos. Sci., 32(1), 32–63, 2015.
Yee, S. K.: Numerical solution of initial boundary value problems involving Maxwell's equations in isotropic media, IEEE Trans. Antennas Propag., 14, 302–307, 1966.
Yi, B., P. Yang, B. A. Baum, T. L'Ecuyer, L. Oreopoulos, E. J. Mlawer, A. J. Heymsfield, and K. N. Liou: Influence of ice particle surface roughening on global cloud radiative effect, J. Atmos. Sci., 70, 2794-2807, 2013.
Yurkin, M. A., Maltsev, V. P., and Hoekstra, A. G.: The discrete dipole approximation for simulation of light scattering by particles much larger than the wavelength. J. Quant. Spectrosc. Radiat. Transfer., 106(1), 546-557, 2007.
Zhang, Z., Yang, P., Kattawar, G., Riedi, J., Labonnote, L. C., Baum, B. A., ... and Huang, H. L.: Influence of ice particle model on satellite ice cloud retrieval: lessons learned from MODIS and POLDER cloud product comparison, Atmos. Chem. Phys., 9, 7115–7129, 2009.

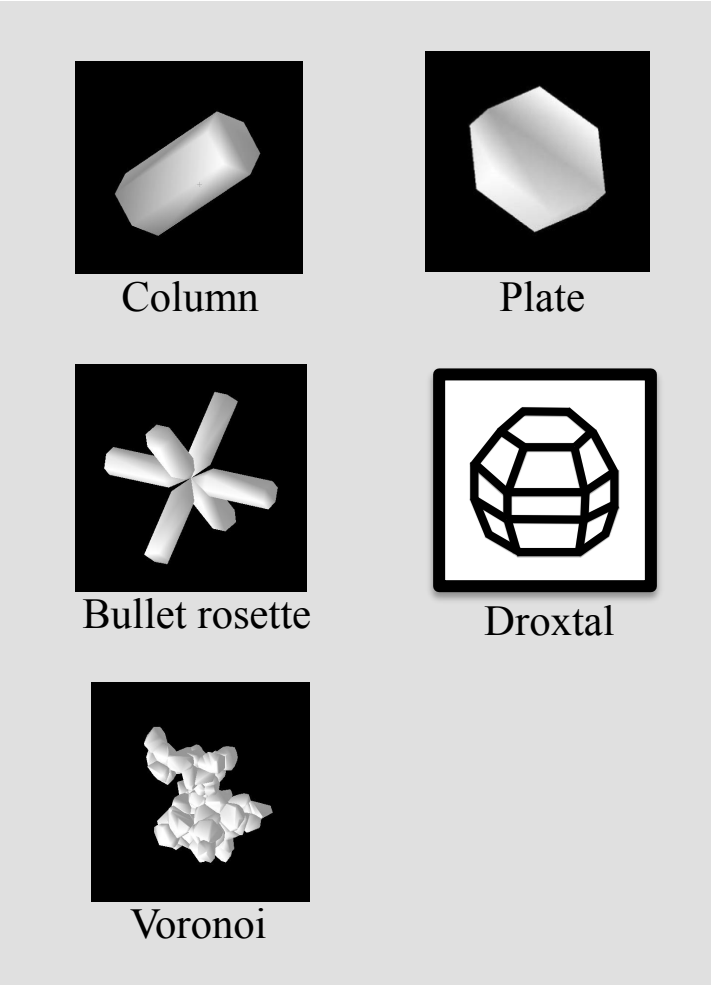

Fig.1 SGLI cloud particle habits

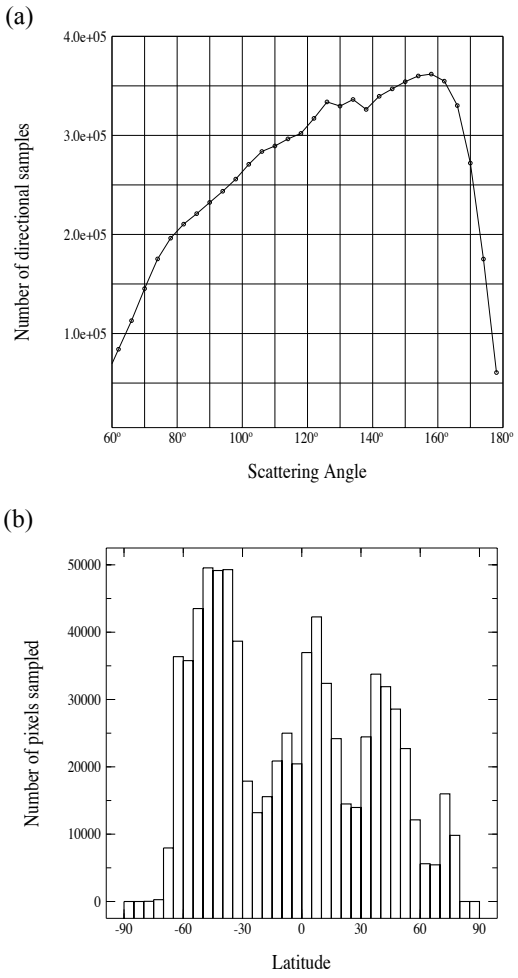

Fig 2. a) Angular distribution and, b) latitude distribution of the sample pixels.

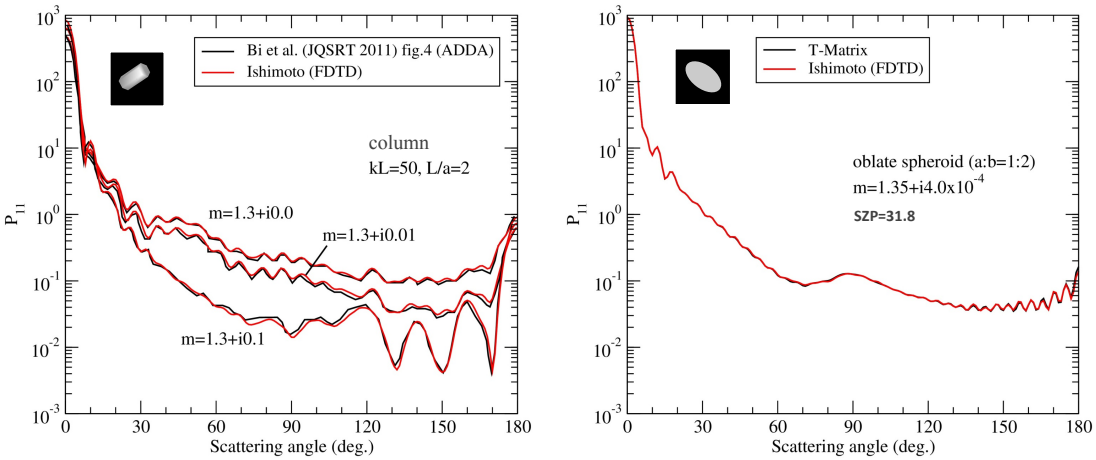

Fig. 3. Comparison of the phase functions of randomly oriented column and spheroid particle from FDTD, T-Matrix and ADDA method.

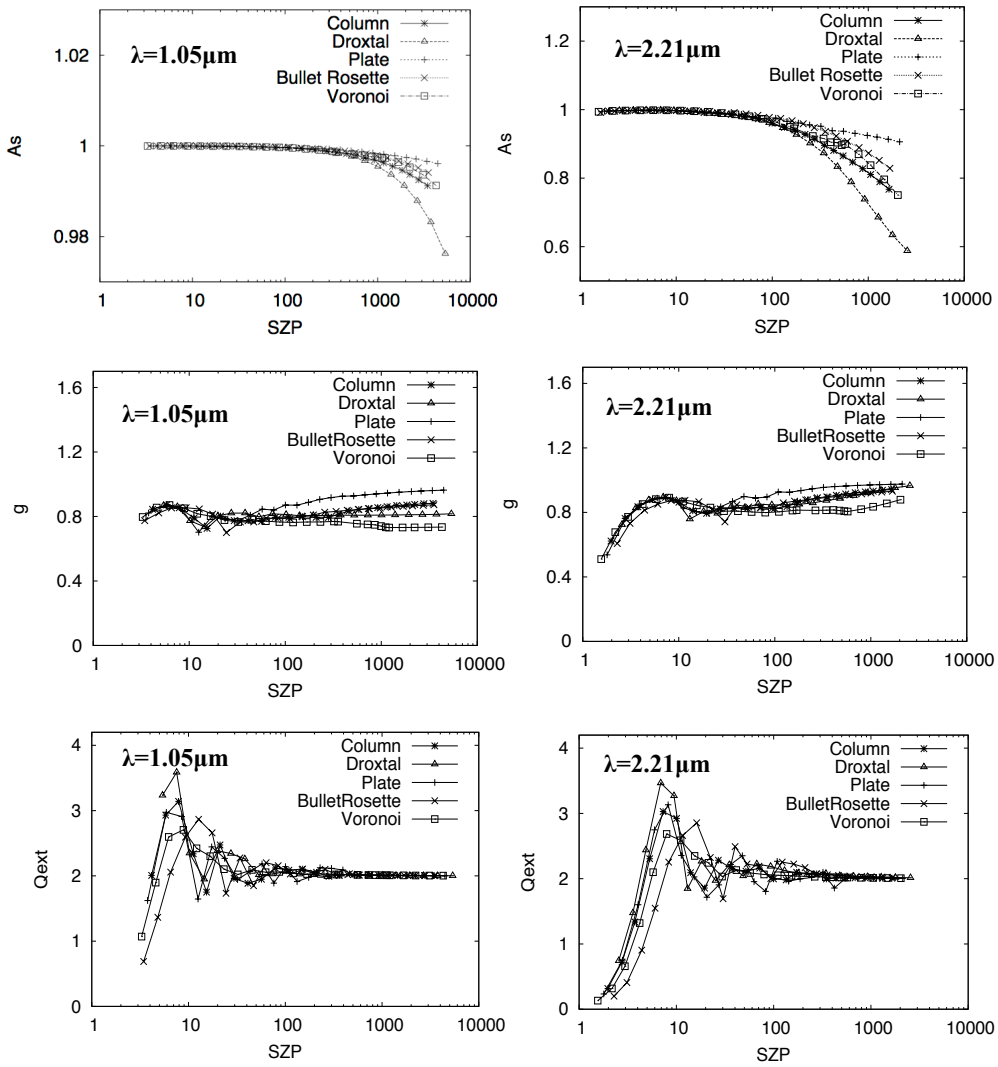

Fig. 4. Comparison of the single scattering property of the various ice crystals models computed in this study at wavelength of 1.05 and 2.21um.

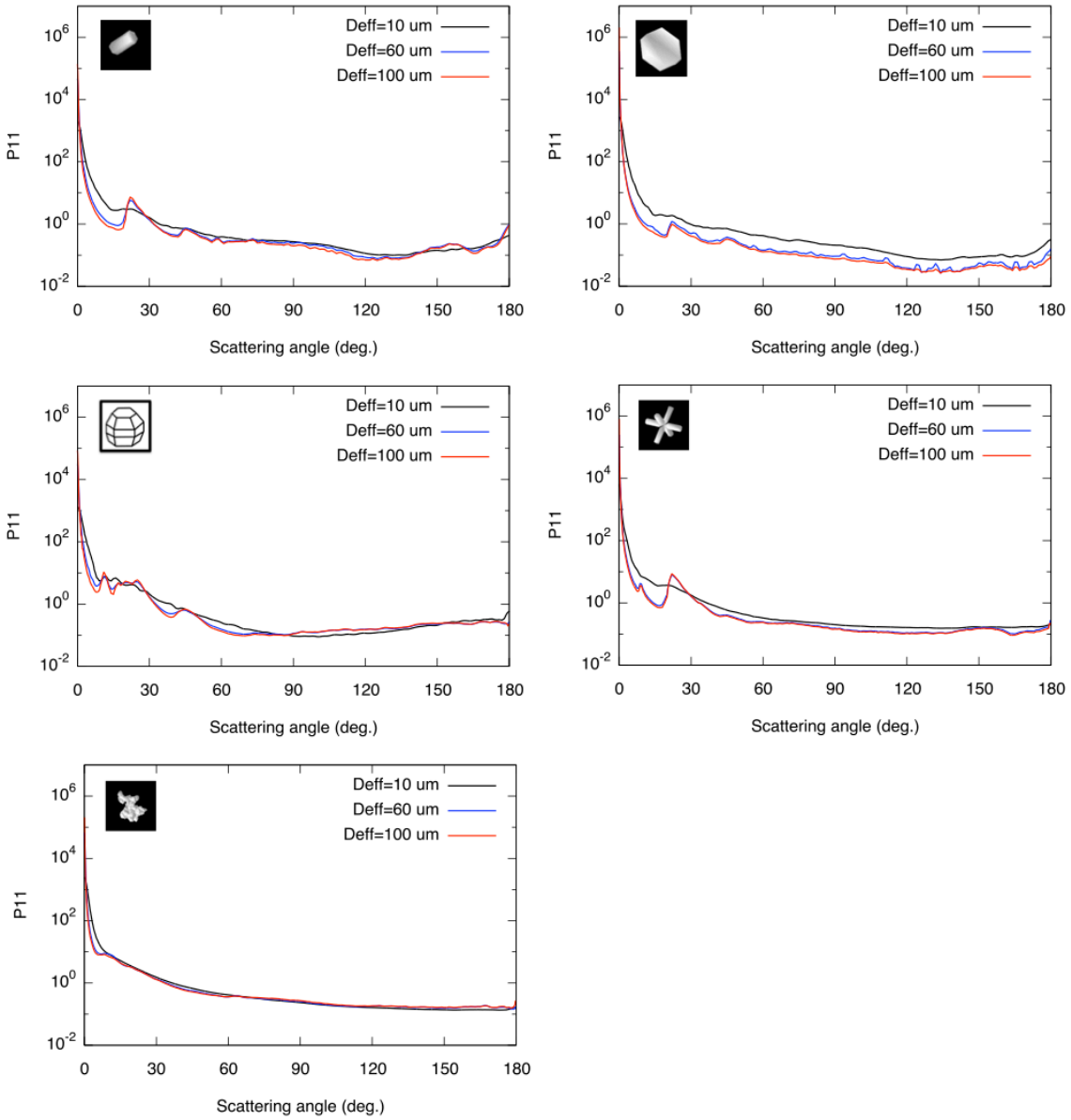

Fig.5. Bulk scattering phase functions of the column, droxtal, plate, bullet rosette and voronoi habit employed in this study with various effective diameters at wavelengths of 1.05 um.

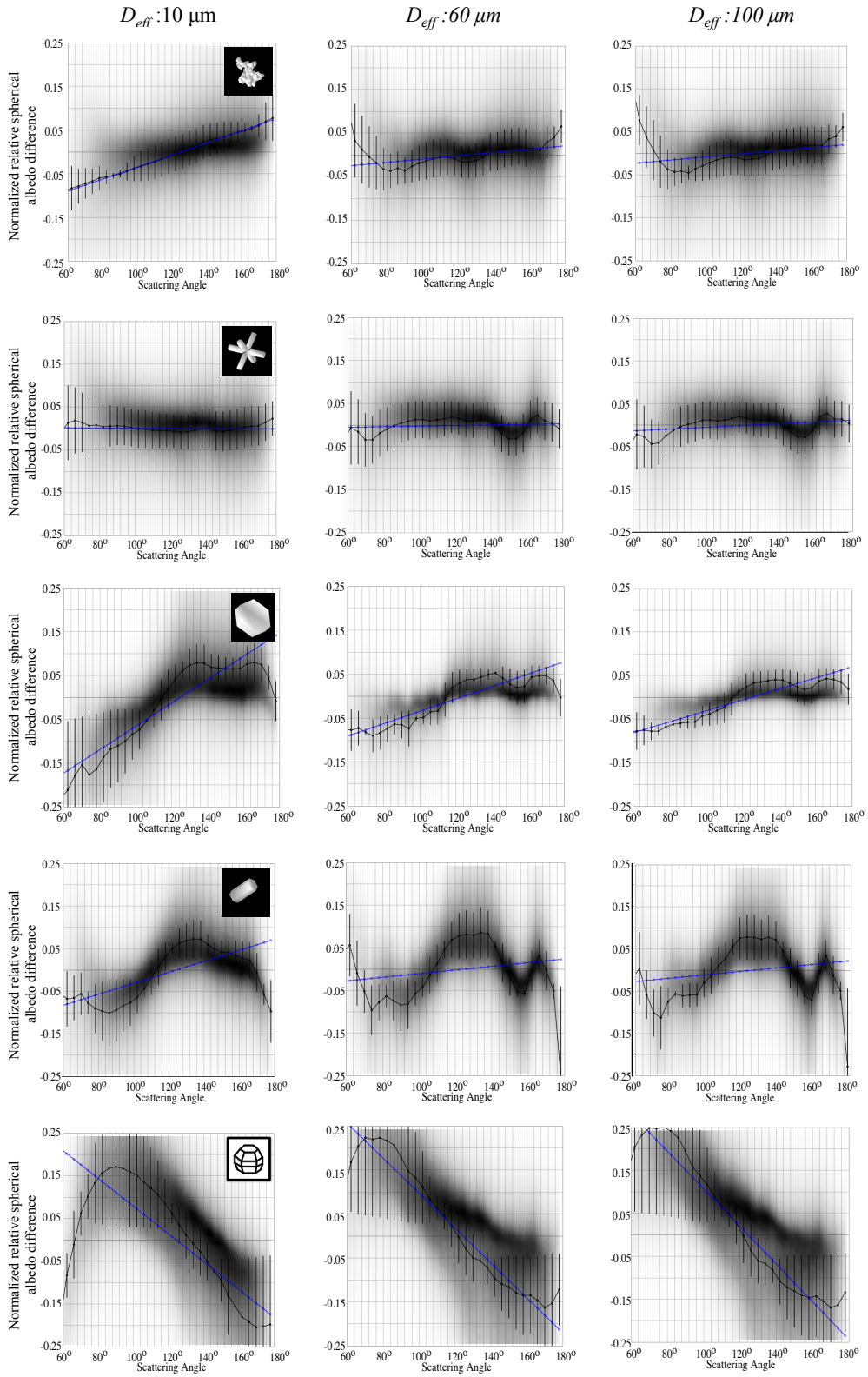

Fig. 6. SAD analysis as a function of different particle habits and effective diameters (D_{eff}) using POLDER measurement. Black contours show the density of the observations normalized to the maximum value, and blue line show the regression line.

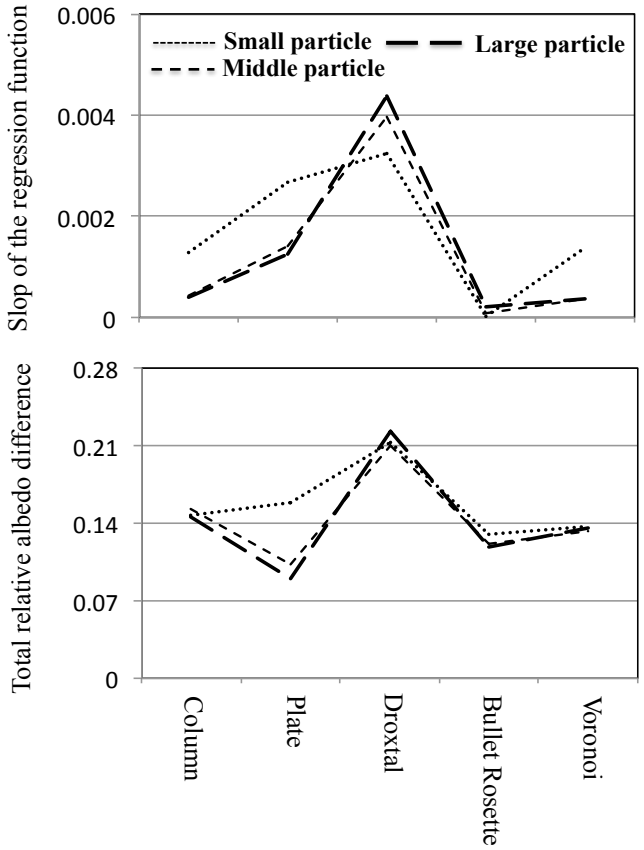

Fig. 7. The slope of the regression function and total relative albedo different in Fig 6.

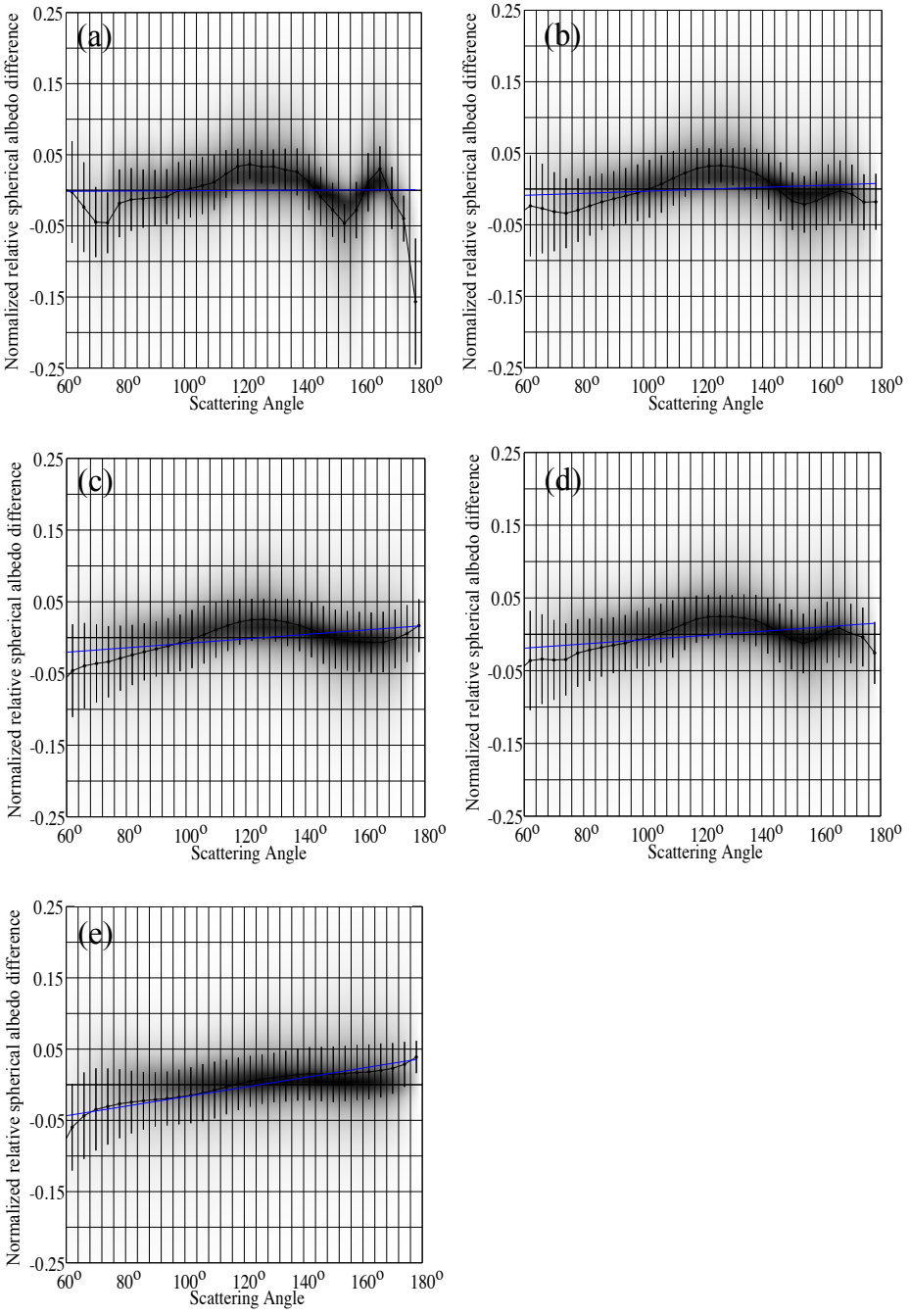

Fig. 8. SAD analysis of the Ensemble ice particle model with D_{eff} =60 μm for various distortions: (a) no distortion applied; (b) with distortion value of 0.15; (c) with distortion value of 0.25; (d) averaged over all distortion values; (e) distortion value of 0.4 is assumed with spherical air inclusions.

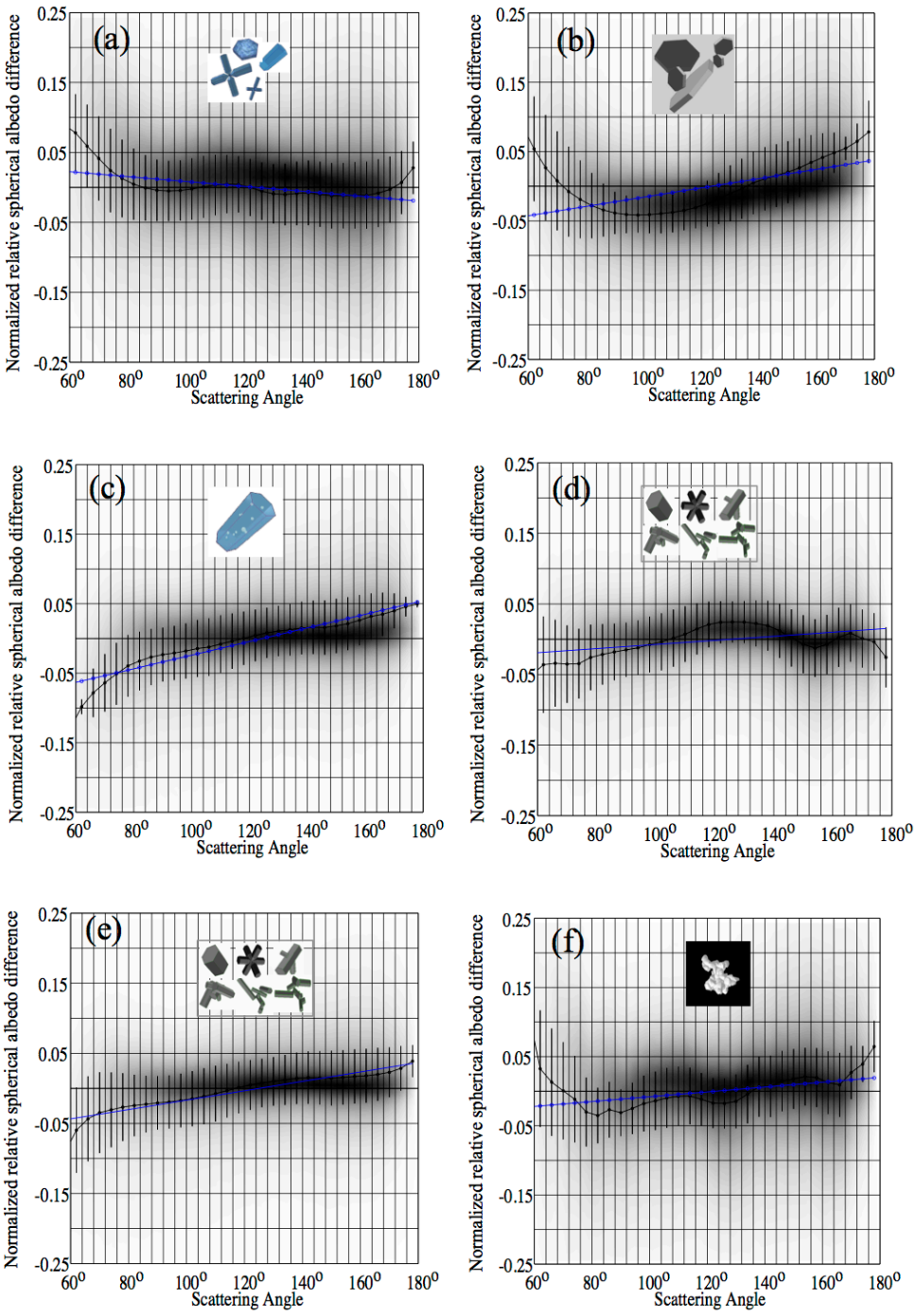

Fig. 9. Comparison of the SAD analysis for various ice particle models with D_{eff} =60 μm : (a) GHM model with rough surface; (b) 5-plate_agr: 5-plate aggregate model with rough surface; (c) IHM model with smooth surface; (d) Ensemble_ave: Ensemble ice particle model with averaged over all distortion value; (e) Ensemble_0.4: Ensemble ice particle model by assuming a distortion value of 0.4 with spherical air inclusions; (f) Voronoi model.

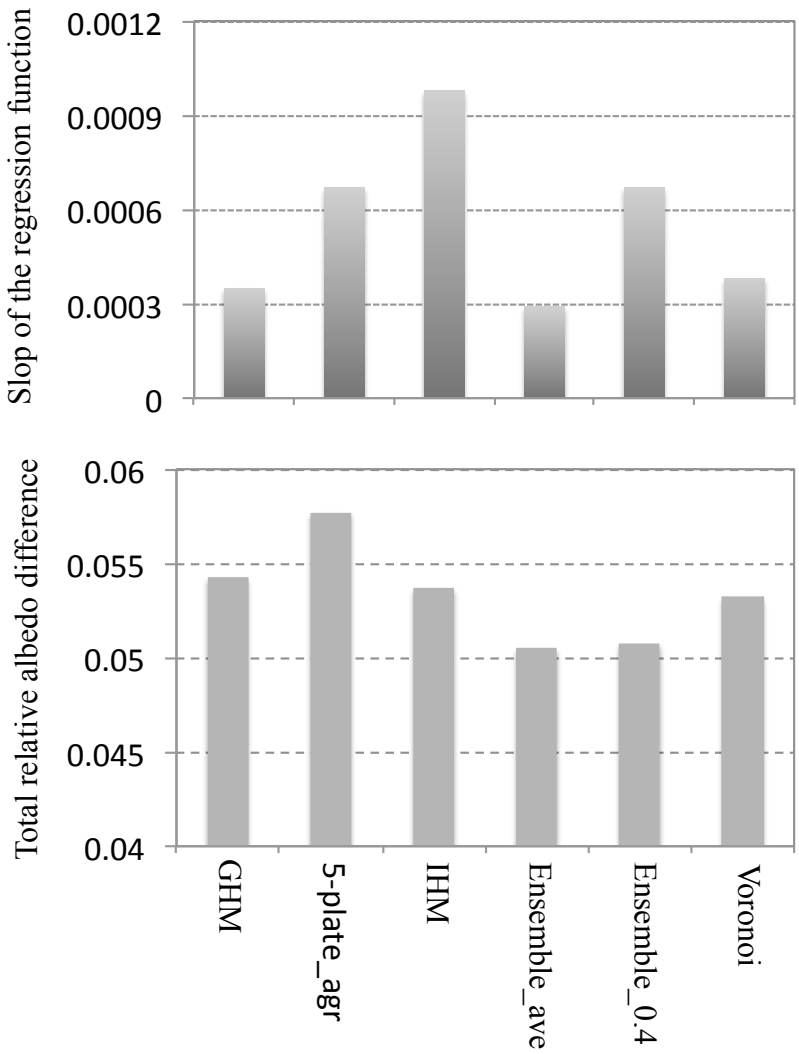

Fig. 10. The slope of the regression function and total relative albedo difference for various ice particle models in Fig 9.

Table 1: Specification of the SGLI

No.	SGLI Channels	Center Wavelength (μm)	Band width (nm)	IFOV (m)
1	VN1	0.380	10	250
2	VN2	0.412	10	250
3	NV3	0.443	10	250
4	NV4	0.490	10	250
5	NV5	0.530	20	250
6	NV6	0.565	20	250
7	NV7	0.673	20	250
8	NV8	0.673	20	250
9	NV9	0.763	12	1000
10	NV10	0.868	20	250
11	NV11	0.868	20	250
12	P1	0.673	20	1000
13	P2	0.868	20	1000
14	SW1	1.050	20	1000
15	SW2	1.380	20	1000
16	SW3	1.630	200	250
17	SW4	2.210	50	1000
18	T1	10.8	740	500
19	T2	12.0	740	500

Table 2: Size parameter with various particle size and calculating wavelength on the SGLI channels (FDTD, GOIE, GOM)

λ(μm) / $\tilde{r}$(μm)	0.5500	0.5650	0.5800	0.6590	0.6740	0.6860	0.8530	0.8650	0.8830
0.700	7.997	7.784	7.583	6.674	6.526	6.411	5.156	5.085	4.981
1.000	11.424	11.121	10.833	9.534	9.322	9.159	7.366	7.264	7.116
1.300	14.851	14.457	14.083	12.395	12.119	11.907	9.576	9.443	9.250
1.900	21.706	21.129	20.583	18.115	17.712	17.402	13.995	13.801	13.520
2.600	29.702	28.914	28.166	24.790	24.238	23.814	19.152	18.886	18.501
3.500	39.984	38.922	37.916	33.370	32.628	32.057	25.781	25.423	24.905
4.900	55.977	54.491	53.082	46.719	45.679	44.880	36.093	35.593	34.867
6.900	78.825	76.733	74.748	65.788	64.323	63.198	50.825	50.120	49.099
9.500	108.528	105.646	102.914	90.577	88.561	87.012	69.977	69.006	67.599
13.200	150.796	146.793	142.997	125.854	123.053	120.901	97.231	95.882	93.928
18.200	207.916	202.396	197.162	173.527	169.665	166.697	134.061	132.201	129.506
25.300	289.027	281.353	274.077	241.221	235.853	231.727	186.359	183.774	180.028
35.100	400.981	390.336	380.241	334.658	327.210	321.487	258.546	254.959	249.762
47.300	540.354	5307.901	5170.628	4550.780	4449.502	4371.668	3515.785	3467.011	3396.336
60.600	692.293	673.913	656.485	577.786	564.927	555.045	446.379	440.186	431.213
77.100	880.788	857.405	835.230	735.104	718.744	706.171	567.917	560.039	548.622
97.500	1113.837	1084.266	1056.225	929.606	908.918	893.018	718.184	708.220	693.783
122.800	1402.864	1365.620	1330.302	1170.827	1144.770	1124.745	904.543	891.994	873.811
154.000	1759.292	1712.585	1668.294	1468.301	1435.624	1410.511	1134.362	1118.625	1095.822
192.700	2201.400	2142.955	2087.534	1837.283	1796.394	1764.971	1419.425	1399.734	1371.200
242.300	2768.029	2694.541	2624.855	2310.191	2258.777	2219.265	1784.778	1760.018	1724.140
308.400	3523.153	3429.618	3340.921	2940.416	2874.977	2824.686	2271.670	2240.155	2194.490
416.380	4756.714	4630.430	4510.677	3969.943	3881.592	3813.692	3067.049	3024.500	2962.846
533.800	6098.117	5936.220	5782.697	5089.475	4976.208	4889.161	3931.963	3877.415	3798.374
	1.0350	1.0500	1.0650	1.3650	1.3800	1.3950	1.4800	1.6300	1.7800
0.700	4.249	4.189	4.130	3.222	3.187	3.153	2.972	2.698	2.471
1.000	6.071	5.984	5.900	4.603	4.553	4.504	4.245	3.855	3.530
1.300	7.892	7.779	7.670	5.984	5.919	5.855	5.519	5.011	4.589
1.900	11.534	11.370	11.209	8.746	8.651	8.558	8.066	7.324	6.707
2.600	15.784	15.558	15.339	11.968	11.838	11.711	11.038	10.022	9.178
3.500	21.247	20.944	20.649	16.111	15.936	15.764	14.859	13.492	12.355
4.900	29.746	29.322	28.909	22.555	22.310	22.070	20.802	18.888	17.296
6.900	41.888	41.290	40.708	31.761	31.416	31.078	29.293	26.598	24.356
9.500	57.672	56.848	56.047	43.729	43.254	42.789	40.331	36.620	33.534
13.200	80.133	78.989	77.876	60.760	60.100	59.454	56.039	50.882	46.594
18.200	110.487	108.909	107.375	83.776	82.865	81.974	77.266	70.156	64.244
25.300	153.589	151.395	149.263	116.458	115.192	113.953	107.409	97.524	89.306
35.100	213.082	210.038	207.080	161.568	159.811	158.093	149.013	135.300	123.899
47.300	2897.550	2856.157	2815.929	2197.043	2173.163	2149.795	2026.327	1839.855	1684.811
60.600	367.885	362.630	357.522	278.946	275.914	272.947	257.271	233.596	213.911
77.100	468.052	461.365	454.867	354.896	351.039	347.264	327.320	297.199	272.154
97.500	591.894	583.439	575.221	448.799	443.921	439.147	413.926	375.835	344.163
122.800	745.483	734.833	724.484	565.257	559.112	553.100	521.335	473.359	433.469
154.000	934.889	921.534	908.554	708.872	701.167	693.628	653.791	593.626	543.601
192.700	1169.826	1153.114	1136.873	887.011	877.369	867.935	818.088	742.804	680.208

242.300	1470.933	1449.920	1429.498	1115.323	1103.200	1091.337	1028.659	933.997	855.290
308.400	1872.207	1845.461	1819.469	1419.586	1404.155	1389.057	1309.280	1188.794	1088.615
416.380	2527.722	2491.612	2456.519	1916.625	1895.792	1875.407	1767.698	1605.026	1469.771
533.800	3240.545	3194.252	3149.262	2457.117	2430.409	2404.275	2266.192	2057.647	1884.250
	2.1730	2.2100	2.2480	10.2450	10.8000	11.3550	11.4450	12.0000	12.5550
0.700	2.024	1.990	1.957	0.429	0.407	0.387	0.384	0.367	0.350
1.000	2.891	2.843	2.795	0.613	0.582	0.553	0.549	0.524	0.500
1.300	3.759	3.696	3.634	0.797	0.756	0.719	0.714	0.681	0.651
1.900	5.494	5.402	5.311	1.165	1.105	1.051	1.043	0.995	0.951
2.600	7.518	7.392	7.267	1.595	1.513	1.439	1.427	1.361	1.301
3.500	10.120	9.951	9.783	2.147	2.036	1.937	1.921	1.833	1.752
4.900	14.168	13.931	13.696	3.005	2.851	2.711	2.690	2.566	2.452
6.900	19.951	19.617	19.286	4.232	4.014	3.818	3.788	3.613	3.453
9.500	27.469	27.009	26.553	5.826	5.527	5.257	5.215	4.974	4.754
13.200	38.168	37.529	36.894	8.095	7.679	7.304	7.247	6.912	6.606
18.200	52.625	51.744	50.869	11.162	10.588	10.071	9.992	9.529	9.108
25.300	73.154	71.930	70.714	15.516	14.719	14.000	13.889	13.247	12.661
35.100	101.491	99.792	98.105	21.527	20.420	19.422	19.270	18.378	17.566
47.300	1380.103	1356.997	1334.059	292.725	277.682	264.110	262.033	249.914	238.866
60.600	175.224	172.290	169.378	37.166	35.256	33.532	33.269	31.730	30.327
77.100	222.933	219.201	215.495	47.285	44.855	42.663	42.327	40.369	38.585
97.500	281.919	277.199	272.514	59.796	56.723	53.951	53.526	51.051	48.794
122.800	355.074	349.129	343.227	75.312	71.442	67.950	67.416	64.298	61.456
154.000	445.288	437.833	430.432	94.447	89.594	85.214	84.544	80.634	77.070
192.700	557.188	547.860	538.599	118.182	112.108	106.629	105.790	100.897	96.437
242.300	700.606	688.876	677.231	148.601	140.964	134.074	133.020	126.868	121.260
308.400	891.732	876.803	861.981	189.140	179.420	170.650	169.308	161.478	154.340
416.380	1203.954	1183.798	1163.787	255.363	242.240	230.400	228.588	218.016	208.379
533.800	1543.472	1517.631	1491.977	327.376	310.552	295.373	293.051	279.497	267.142